ChemComm

FEATURE ARTICLE

View Article Online
View Journal | View Issue

Cite this: *Chem. Commun.*, 2015, **51**, 16014

Received 9th September 2015,
Accepted 6th October 2015

DOI: 10.1039/c5cc07513k

www.rsc.org/chemcomm

π-Electron rich small molecule sensors for the recognition of nitroaromatics

Sankarasekaran Shanmugaraju and Partha Sarathi Mukherjee*

Selective and discriminative detection of $-NO_2$ containing high energy organic compounds such as picric acid (PA), 2,4,6-trinitrotoluene (TNT) and dinitrotoluene (DNT) has become a challenging task due to concerns over national security, criminal investigations and environment protections. Among various known detection methods, fluorescence techniques have gained special attention in recent time. A wide variety of fluorescent chemosensors have been developed for nitroaromatic explosive detection. In this review article, we provide an overview of the recent developments made in small molecule-based turn-off fluorescent sensors for nitroaromatic explosives with special focus on organic and H-bonded supramolecular sensors. The fluorescent sensors discussed in this review are classified and organized according to their functionality and their recognition of nitroaromatics by fluorescence quenching.

1. Introduction

Fast and reliable chemical sensors for the trace detection of hazardous chemical species have attracted special attention in recent years due to their possible applications in environmental cleaning and home land security.[1] Polynitro aromatic compounds (NACs) such as picric acid (PA), 2,4,6-trinitrotoluene (TNT) and its degradation product dinitrotoluene (DNT) are used as primary constituents of many known chemical explosives.[2] For instance, tritonal is a known chemical explosive comprised of 80% TNT and 20% Al powder.[3] In addition to their high explosive nature, there are many health concerns relating to nitroaromatics. Excess inhalation of TNT may cause abnormal liver function and also may lead to severe neurological damage.[4] According to US Environmental Protection Agency (EPA), the permissible level of TNT in drinking water is ~2 ppb and above this level it is considered to be toxic.[5] Therefore, suitable sensors with high sensitivity and discriminating ability for the trace identification of NACs in soil, groundwater, and land mine areas have high demand. Currently, a wide range of instrumental techniques like metal detection, surface-enhanced Raman spectroscopy (SERS), gas chromatography-mass spectrometry

Department of Inorganic and Physical Chemistry, Indian Institute of Science, Bangalore 560012, India. E-mail: psm@ipc.iisc.ernet.in; Fax: +91-80-2360-1552; Tel: +91-80-2293-3352

Sankarasekaran Shanmugaraju

Sankarasekaran Shanmugaraju obtained his BSc and MSc degrees in Chemistry from The American College, Madurai. After this he completed a PhD in inorganic Chemistry in 2013 under the supervision of Prof. Partha Sarathi Mukherjee at Indian Institute of Science-Bangalore. His PhD thesis was selected for Prof. S. Soundarajan best thesis award (gold medal). His research interests are on self-assembly of supramolecular functional materials and small molecule based chemosensors.

Partha Sarathi Mukherjee

Partha Sarathi Mukherjee received his PhD working with Prof. N. Ray Chaudhuri at the Indian Association for the Cultivation of Science (IACS), and his postdoctoral from University of Utah with Prof. Peter J. Stang. In 2004, he moved to University of Gottingen to work with Prof. Herbert W. Roesky as an AvH fellow. He has been at the Indian Institute of Science, Bangalore, since July 2005, where he is currently an Associate Professor. His current research interests are in the areas of self-assembly of functional molecular architectures and supramolecular chemistry.

(GC-MS), X-ray diffraction, nuclear quadrupole resonance (NQR), cyclic voltammetry, *etc.* are available for NAC detection.[6] However, the real-time use of these methods is being limited due to their expensive instrumentation, lack of portability and difficult operation on-site. In recent years, however, the fluorescence techniques have become alternative detection methods for nitro-explosive detection owing to high sensitivity, quick responses and portability of these techniques.[7] In fluorescence-based sensing methods, the initial emission intensity of fluorophores is perturbed (quenched or enhanced) upon binding with analytes.[8] In light of this, over the past decade, a wide variety of fluorescent sensors like conjugated organic/inorganic polymers,[9] molecularly imprinted polymers (MIPs),[10] porous metal–organic frameworks (MOFs),[11] covalent organic polymers (COPs),[12] discrete macrocycles/cages,[13] luminescent gels,[14] organic–inorganic hybrid materials,[15] dendrimers,[16] quantum dots,[17] *etc.* have been developed and screened for NAC detection. However, in addition to the aforesaid fluorescent sensors, the interest has been directed towards the design of simple π-electron-rich small molecule fluorescent sensors for NAC detection.[18]

Small molecule based fluorescent sensors are attractive in terms of their straightforward synthesis, easy purification, better reproducibility and high quantum yield.[19] An added advantage is their easy chemical modification by introducing suitable functional groups to increase the sensing selectivity and sensitivity. Moreover, unlike metal–organic frameworks (MOFs) and many polymers, small molecule based sensors are mostly soluble in common solvents, which makes them very easy to fabricate for practical applications. In general, turn-on fluorescent sensors for explosive detection are more appealing because analyte binding leads to a significance enhancement of emission intensity and thus sensing may be easily visualized by the naked eye.[20] However, the design of turn-on fluorescent sensors is very complicated and also limited for real-time application due to their very small Stoke's shift and lack of reversibility. Therefore, in recent years the interest has been directed towards the design of turn-off fluorescent sensors. Until recently, a plethora of small molecule-based fluorescent chemosensors have been designed, synthesized and successfully employed for NAC detection both in solution and vapor-phase.[20,21] Although several articles highlighting the nitroaromatic sensing ability of various materials (organic/inorganic polymers, MOF, fluorescent nanofibrils, *etc.*) have been reported recently, the present review is dedicated mainly on NAC sensing by π-electron-rich small molecule based fluorescent sensors.[1,2,9a,g,10,11,14a,18a,22] We aim to provide an overview of fluorescent turn-off chemosensors and particular emphasis is given to poly-(hetero)cyclic aromatic hydrocarbons for nitroaromatic explosive detection. The chemical structures of nitroaromatics and other interfering analytes considered in this review article are depicted in Chart 1.

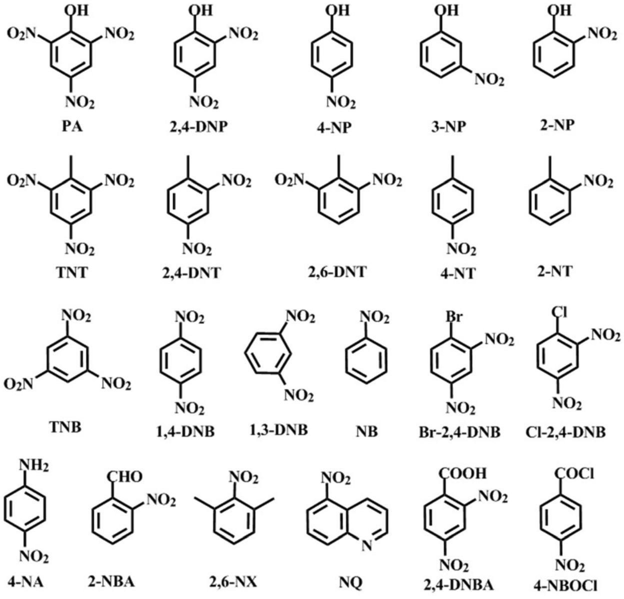

Chart 1 Nitroaromatic analytes discussed in this review.

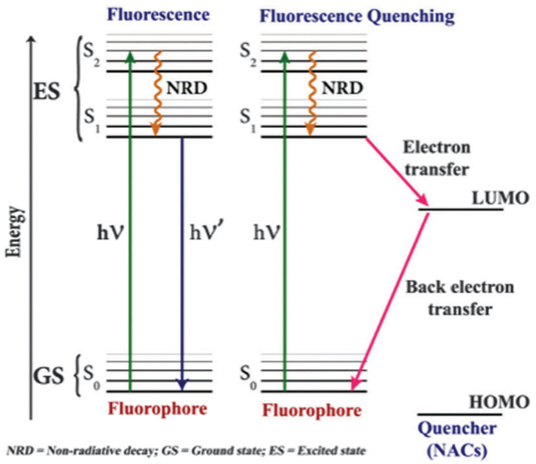

Fig. 1 Energy level diagram for electron-transfer fluorescence quenching.

In fluorescence quenching based detection of explosives, the initial fluorescence intensity of a fluorophore decreases in presence of an analyte and in general it follows two different mechanistic pathways static quenching and collisional quenching (Fig. 1).[7a] Both static and collisional fluorescence quenching are often achieved through simple electron transfer processes from the photo-excited fluorophore (acting as an electron-donor) to the ground state NAC (act as an electron-acceptor).[2] In the static mechanism, the fluorophore generally binds with the analyte in the ground state *via* non-fluorescent complex formation and it solely depends on the binding of the analyte to the fluorophore. In contrast, collisional quenching is an excited state process in which the analyte binds with the fluorophore in the excited state and it depends on the rate of collision between the analyte and the fluorophore as well as the lifetime of the fluorophore.[22] Hence, the mechanism of fluorescence quenching can be distinguished by monitoring the intrinsic fluorescence lifetime of the fluorophore as a function of the quencher concentration. The static and collisional fluorescence quenching are often characterized by a linear Stern–Volmer plot which is a direct measure of quenching efficiency and sensitivity.[22,23] The details of the mechanism of fluorescence quenching, quenching efficiency and selectivity of small molecule fluorophores considered in this review article are highlighted in the following sections.

2. Pyrene based sensors

In recent years, pyrene and its derivatives have drawn substantial attention as fluorescent tags/probes in various applications due to their interesting photo-physical properties, high stability and planar aromatic surface which tend to form strong charge-transfer complexes with electron-deficient analytes (Chart 2). In 2001, Goodpaster and McGuffin demonstrated the phenomenon of selective fluorescence quenching of free pyrene **1** as an indirect detection method in combination with mass-spectrometry/gas-chromatography for TNT and its derivatives.[24] The free pyrene **1** showed selective fluorescence quenching for NACs with Stern–Volmer quenching constants of K_{SV} = 307–394 M^{-1}. Chen *et al.* reported the efficacy of 1-bromopyrene **2** as a fluorescence probe for NACs.[25] Despite the heavy atom effect of the -Br atom, 1-bromopyrene (**2**) exhibited an intense emission in dimethylformamide (DMF) solution and the emission was quenched significantly in presence of NACs with quenching constants in the order of 1–3 × 10^3 M^{-1}.

In 2011, Mukherjee *et al.* reported a pyrene based fluorescent sensor **3** substituted with bulky-trimethylsilylethynyl (TMS) groups for parts per billion (ppb) level detection of NACs.[26] Among the nitroaromatics and other aromatics, TNT (K_{SV} = 1.4 × 10^3 M^{-1}) and PA (K_{SV} = 1.1 × 10^3 M^{-1}) showed the highest level of fluorescence quenching towards sensor **3** including sharp visual color changes (Fig. 2). In addition, the freshly made thin film of **3** also displayed efficient and differential fluorescence quenching responses towards the saturated vapors of NACs and the observed quenching is basically reversible. Fluorescence quenching efficiencies of nearly 50% for nitrobenzene (NB), 46% for 4-nitrophenol (4-NP) and 25% for 4-nitrotoluene (4-NT) were observed upon 120 s exposure of the thin film of **3** and the reason for the observed difference in the quenching efficiency surmised to the difference in vapor pressure and redox potential (Fig. 2). It is noteworthy that exposure of the film of **3** to the vapors of other analytes like benzoic acid (BA), benzoquinone (BQ) and anthraquinone (AQ) elicited little enhancement in intensity.[26]

In 2013, the same group reported two π-electron-rich pyrene functionalized sensors **4** and **5** attached with bulky 2-methyl-3-butyn-2-ol groups.[27] Compounds **4** and **5** were synthesized in high yields by employing Sonogashira coupling between the corresponding aryl-halides and 2-methyl-3-butyn-2-ol. Due to the extended π-conjugation, **4** and **5** showed a strong fluorescence emission and showed very high quenching responses with moderate selectivity for NACs such as TNT, 2,4-dinitrotoluene (2,4-DNT) over various other electron deficient/rich aromatic analytes. The calculated quenching constants

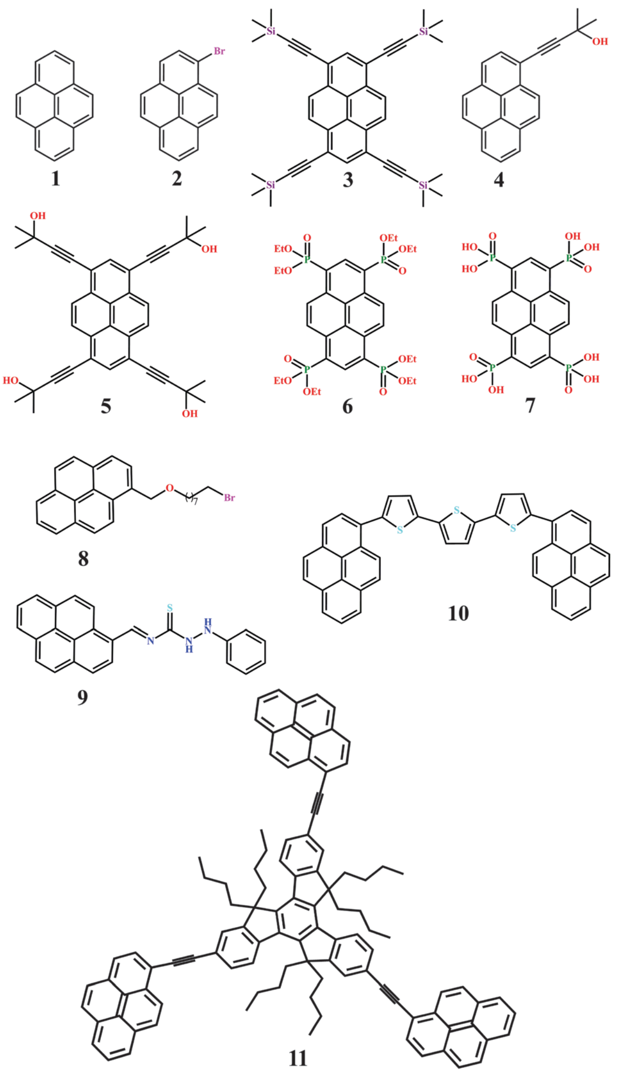

Chart 2 Examples of a few pyrene based sensors.

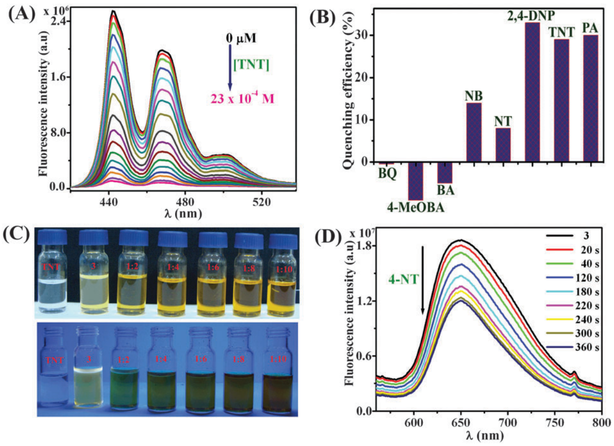

Fig. 2 (A) Fluorescence quenching of **3** upon gradual addition of TNT in $CHCl_3$; (B) relative changes in fluorescence intensity of **3** upon addition of various analytes; (C) visual color changes observed upon treating 17 mM solution of **3** with increasing quantity of TNT (1 to 10 equivalents) in $CHCl_3$; (D) fluorescence quenching of the thin film of **3** upon exposure to the saturated vapor of 4-NT at different time intervals. Adapted with permission from ref. 26. Copyright 2011 Royal Society of Chemistry.

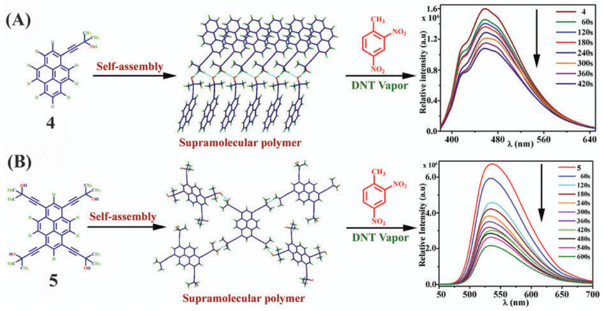

Fig. 3 (A) Supramolecular self-assembly of **4** in solid-state and fluorescence quenching of the thin film of **4** upon exposure to the saturated vapor of 2,4-DNT at different time intervals. (B) Supramolecular self-assembly of **5** in solid-state and fluorescence quenching of the thin film of **5** upon exposure to the saturated vapor of 2,4-DNT at different time intervals. Adapted with permission from ref. 27. Copyright 2013 Royal Society of Chemistry.

(K_{SV}) from the titration profile were 1.9×10^2 M^{-1} for **4** with TNT; 6.4×10^3 M^{-1} for **5** with TNT and 1.3×10^2 M^{-1} for **4** with 2,4-DNT; 3.9×10^3 M^{-1} for **5** with 2,4-DNT. The observed relatively poor fluorescence quenching responses of **4** were attributed to its less π-conjugation than **5**. The solid-state packing of **4** in the crystalline state exhibited a strong H-bonded (1.97 Å) 1D chain and the neighboring chains are mutually stacked to adopt a zig-zag 2D network *via* CH–π interactions (2.85 Å). Sensor **5** formed a 3D supramolecular porous network *via* only H-bonding (1.95 Å) interactions (Fig. 3). Furthermore, 360 s exposure of a freshly made thin film of **5** to saturated 2,4-DNT vapor caused ∼55% quenching of intensity and quenching efficiency increased to 67% after 6 min of exposure. On the other hand, the thin film of **4** exhibited only 31% quenching for 360 s exposure to 2,4-DNT vapor (Fig. 3). The better quenching efficiency of **5** was ascribed to the rapid diffusion of analytes within the intrinsic microporous structure of the 3D supramolecular polymer.[27]

Recently, Venkatramaiah *et al.* described a new class of phosphonate functionalized pyrene-based fluorescent compounds **6** and **7** for NAC detection.[28] The covalent attachment of P═O groups on the periphery of pyrene stabilizes the LUMO of **6** and **7** through d_π–p_π overlapping and thus facilitate the efficient electron-transfer from sensors to NACs. Furthermore, the presence of phosphoryl groups prevents the aggregation of sensors in solution due to the steric hindrance and the unprotected –OH group in **7** further acts as a receptor for NACs through H-bonding interactions. Both the sensors (**6** and **7**) showed monomer pyrene emission centered at $\lambda = 387$ nm with lifetimes of 3.74 ns (**6**) and 3.42 nm (**7**), while the fluorescence quantum yields were 36% for **6** and 22% for **7** in solution. In contrast, spin-coated thin films showed broad excimer emission bands at 505 nm (**6**) and 515 nm (**7**) with Stokes shifts of 132 nm (**6**) and 140 nm (**7**). The emission intensity of **6** and **7** in solution depleted gradually (82% for **6** and 91% for **7**) upon addition of TNT with a detection limit of 2–14 ppb, while the addition of PA quenched 51% (**6**) and 74% (**7**) of intensity. The high quenching efficiency of **7** was attributed to the strong π–π interactions as well as H-bonding between the sensor and NACs. The calculated K_{SV} were 8.4×10^4 M^{-1} for **7** with TNT; 3.6×10^4 M^{-1} for **7** with PA; 6.6×10^4 M^{-1} for **6** with TNT and 2.9×10^4 M^{-1} for **6** with PA. Notably, the non-perturbation in emission intensity upon addition of other NACs and some other volatile organic compounds evidenced that both sensors **6** and **7** displayed a preferential binding with TNT and PA in solution. Further, the emission intensity of the thin film of **7** quenched significantly to 30% in 30 s exposure to TNT vapor and increased to 93% after 180 s exposure, while the thin film of **6** exhibited 86% quenching in 360 s. Exposure of films to saturated vapors of other tested analytes elicited poor quenching. The authors concluded that the phosphonate functionalized pyrene derivatives could be new materials with superior sensitivity and selectivity for NACs.[28]

A pyrene based sensor **8** showed two monomeric emissions at 378 nm and 398 nm and one broad excimer emission at 484 nm.[29] The addition of TNT to the solution of **8** in CTAB micelles caused a decrease in intensity of both monomer and excimer emissions. The observed large quenching constant ($K_{SV} = 2.9 \times 10^5$ M^{-1}) was attributed to the hydrophobic nature of **8**. Chemosensor **9** based on pyrene-linked with thiourea was synthesized and used as a selective probe for PA over other NACs in solution.[30] Sensor **9** was synthesized by a simple condensation reaction between *N*-phenylthiosemicarbazide and pyrene-1-carboxaldehyde in ethanol. The strong fluorescence emission of **9** ($\Phi = 0.045$) was quenched ($\Phi = 0.015$) completely including a sharp visual color change from pale yellow to green in the presence of up to 2 equiv. of PA which resulted in the non-fluorescent complex (1 : 1) formation. The detection limit was found to be 2.0×10^{-7} M^{-1} and the binding constant was calculated to be $K_{SV} = 4.0 \times 10^6$ M^{-1}. The addition of other NACs such as 4-nitroaniline (4-NA), 2-nitrophenol (2-NP), NB, 2-nitrobenzaldehyde (2-NBAl), 1-bromo-2-nitrobenzene (Br-2NB), 4-nitrobenzoylchloride (4-NBOCl) elicited no fluorescence quenching.[30]

In 2013, Fang *et al.* synthesized a novel terthiophene–pyrene conjugate (**10**) employing Grignard reaction and screened it as a selective probe for NACs.[31] Solution state fluorescence studies demonstrated that conjugate **10** was highly sensitive to the presence of NACs, in particular for PA with a detection limit of 6.21×10^{-7} mol L^{-1}. On the other hand, the quenching efficiencies of 3.0×10^{-3} mol L^{-1} solutions of NB, TNT and 2,4-DNT for emission intensity of **10** were 59.4%, 37.9% and 29.2%, respectively, whereas, the commonly known interference including benzene (Bz), toluene (Tl) and BA induced little quenching effects on the emission.[31]

Very recently, a star-shaped truxene-based fluorescent sensor **11** containing three ethynyl-pyrene units at peripheries was synthesized and demonstrated to be a selective sensor for NACs.[32] The truxene functionality was chosen as the core unit owing to its well-defined and rigid structure as well as high thermal stability and strong emissive nature. The attachment of ethynyl-pyrene functionality increased the extended π-conjugation and served as primary binding sites for NACs. The substitution of *n*-butyl alkyl chains to the core truxene unit prevented the intermolecular π–π stacking and increased the solubility of compound **11** in common solvents. Compound **11** showed two emission maxima at 415 nm and 442 nm in $CHCl_3$ with a calculated quantum yield of 71% and this was decreased to 53% upon addition of 10% H_2O in THF medium, which indicated that sensor **11** self-aggregated in mixed aqueous solution. The emission intensity of **11** in $CHCl_3$ solution was quenched in the presence of 2-NP with a Stern–Volmer constant of $K_{SV} = 3.2 \times 10^3\ M^{-1}$ and the detection limit was 1.54 ppm, whereas, the aqueous THF solution (10% H_2O in THF) of **11** selectively binds ($K_{SV} = 3.6 \times 10^4\ M^{-1}$) with PA with a detection limit of 0.15 ppm. The observed fluorescence quenching followed the static quenching mechanism in which the electron-rich pyrene moiety binds with electron-poor NACs through π–π interactions.[32]

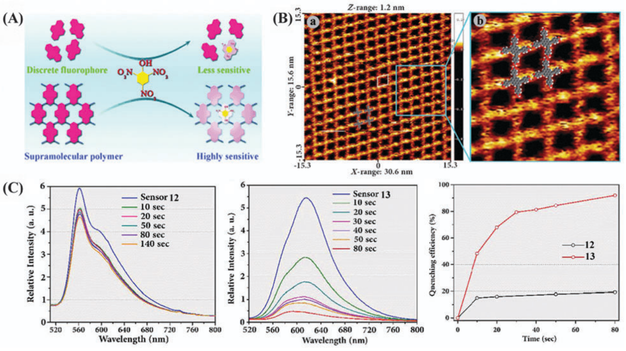

Fig. 4 (A) Schematic representation of the fluorescence quenching mechanism using discrete fluorophores and their extended supramolecular networks. (B) The STM image of sensor **13** self-assembled at the nonanoic acid–graphite interface indicating the intermolecular hydrogen bonding between the carboxylic acid groups. (C) Time dependent fluorescence quenching of thin films of sensors **12** (left) and **13** (middle) using saturated vapour of NB and their corresponding quenching efficiency plots (right). Adapted with permission from ref. 33. Copyright 2014 Wiley-VCH.

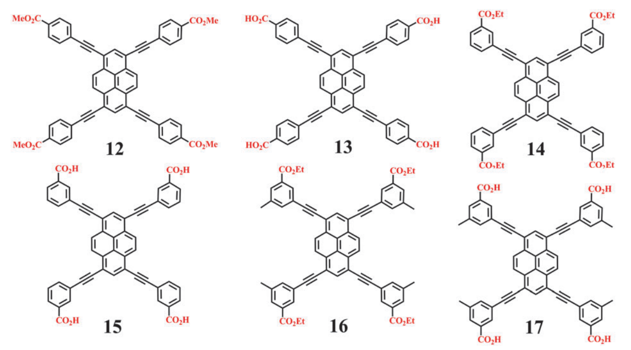

Chart 3 Pyrene functionalized tetracarboxylic acids and their esters analogous.

In 2014, Mukherjee and coworkers designed a series of X-shaped pyrene functionalized fluorescent sensors **12–17** and demonstrated their binding propensity towards NACs both in solution and vapour phase.[33] Compounds **12**, **14** and **16** with ester functionalities were synthesized by a Sonogashira coupling between 1,3,6,8-tetrabromopyrene and corresponding alkyne derivatives and subsequent base hydrolysis yielded their acid analogues of **13**, **15** and **17** (Chart 3). Compounds **12–17** were highly emissive and displayed both monomer (∼490 nm) and excimer (∼520 nm) emissions. Notably, the emission bands of acids were slightly red-shifted compared to their ester analogues due to the supramolecular aggregates formation in solution. The initial emission intensity of all these sensors decreased upon gradual addition of NACs and compounds with –COOH groups and displayed higher and fast fluorescence quenching responses with moderate selectivity compared to their ester analogues. The calculated quenching constants from the PA titration profile were $9.9 \times 10^3\ M^{-1}$ (**12**); $2.2 \times 10^4\ M^{-1}$ (**13**); $1.1 \times 10^3\ M^{-1}$ (**14**); $3.2 \times 10^4\ M^{-1}$ (**15**); $8.1 \times 10^3\ M^{-1}$ (**16**) and $3.7 \times 10^4\ M^{-1}$ (**17**). The titration studies also showed that all these compounds could detect PA and TNT even at parts per trillion (ppt) levels. Furthermore, exposure of thin films of all these sensors to the vapors of different NACs caused depletion of emission intensity. The emission intensity of a film of **12** quenched ∼19% after exposure to NB for 140 s, while a film of **13** attained almost 90% fluorescence quenching in just 80 s exposure at room temperature (Fig. 4). The observed higher and fast fluorescence quenching responses of **13**, **15** and **17** were ascribed to their facile self-aggregation through intermolecular H-bonding interactions which led to a higher long-range exciton migration along the molecular backbone (Fig. 4). On the other side, relatively poor quenching responses of **12**, **14** and **16** were due to their discrete nature. The self-association of –COOH adorned sensors was explained in solution by concentration dependent titrations including dynamic light scattering studies and in solid-state using STM microscopy (Fig. 4). To sum-up, the efficient sensing ability and high selectivity for NACs including the ppt level of sensitivity make the fluorophores **12–17** potential materials for sensing.[33]

The design of clip-type molecular sensors (Chart 4) has become an area of growing interest because of their open cavity capable of binding guest molecules through multiple supramolecular interactions and is subsequently expected to show superior binding affinity for analyte detection.[34] Accordingly, Cho and

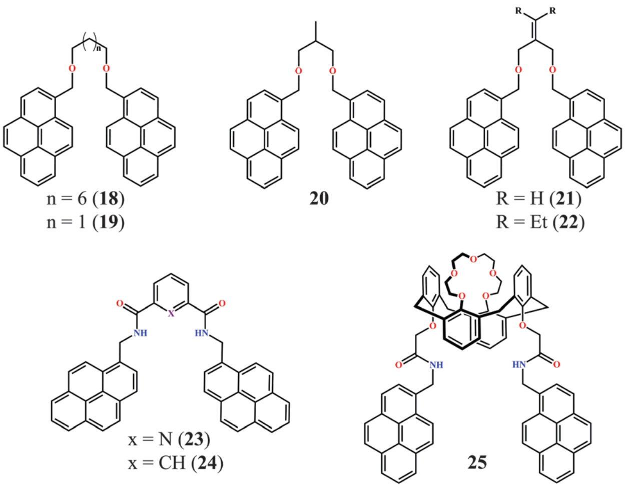

Chart 4 Examples of a few clip-type compounds as sensors for nitroaromatics.

co-workers synthesized a simple dipyrenyl ''clip'' (**18**) that can sense NACs effectively in CTAB micelles *via* charge-transfer complex formation.[29] The semi-empirical PM3 calculation revealed that **18**, due to a smaller size, is easily being accommodated within the CTAB core size of 23.145 Å. Due to the enforced hydrophobic cavity in CTAB micelles, compound **18** showed strong excimer as well as monomer emissions, which were quenched effectively upon addition of NACs. Nearly 45% quenching efficiency was observed even at a concentration of 1.0 equivalent of TNT. The estimated binding constant was $K_a = 1.0 \times 10^6\ \mathrm{M}^{-1}$ in the presence of 1.55 mM of TNT in CTAB micelle medium. The observed higher binding propensity of **18** for TNT compared to other similar sensors was due to the enforced residence or inclusion of **18** in the CTAB micelle medium. The Job's plot analysis indicated that **18** binds TNT in a 1 : 1 stoichiometry within its molecular cleft and also showed that sensor **18** can detect <2 ppb level of TNT including its (<2.6 ng) visual detection using a hand-hold UV lamp. In addition, similar titrations with other NACs such as 2,6-DNT, 1,3-DNB and NB caused poor quenching effects than TNT.[29]

In 2013, the same group reported a series of analogous dipyrenyl sensors (**19–22**). The compounds were synthesized employing a simple substitution reaction between diols and 1-(bromomethyl)pyrene and were used to detect the trace quantity of NACs through hydrophobic interactions and steric constrains in semi-aqueous medium.[35] Fluorescence titration of the receptors **19–22** also displayed a very strong charge-transfer complex formation like **18** and subsequent fluorescence quenching. The calculated Stern–Volmer binding constants followed the order **21** ≥ **20** > **19** > **22** > **18**. The larger binding constant of **19** over **18** was ascribed to the shorter chain length, which required less preorganization energy to form donor–acceptor complexation with NACs. The binding efficiency was further increased either by just introducing a methyl ($-CH_3$) group (**20**) or a double bond (**21**) in the backbone between two pyrene moieties. Among these, compound **21** showed the highest binding affinity for NACs owing to the conformational strain of its double bond, which helped the two pyrenyl units to align perfectly parallel to embrace TNT. In spite of the large steric strain caused by two substituted $-CH_3$ groups, compound **22** showed less binding affinity with TNT because the pyrenyl groups were not parallel to each other, which was supported by AM1 energy minimization; thereby destabilized the CT complex formation. The Job's plot indicated a 1 : 1 donor–acceptor complex formation between **21** and TNT. Among various other NACs, only TNT displayed the greatest quenching efficiency with sensor **21** ($K_{SV} = 409\,900 \pm 18\,900$) and the estimated detection limit was <2 ppb in drinking water.[35]

Sessler and co-workers designed two similar molecular ''clip'' receptors bearing pyridine (**23**) or phenyl (**24**) moieties with the pyrene chromophore linked through the amide functionality.[36] The pyridine containing receptor **23** adopted a supramolecular oligomeric structure mainly through pyridine-N and amide-NH hydrogen bonding and other multiple interactions both in $CHCl_3$ solution as well as in solid-state. In contrast, the phenyl containing receptor **24** did not form such supramolecular structures due to the lack of crucial intermolecular (NH···N) hydrogen bonding interactions. The formed linear supramolecular array of **23** was de-aggregated upon exposure to electron-deficient substrates such as TNB and TNT that led to the formation of simple 1 : 1 donor–acceptor complexes. Notably, the subsequent mixing of methanol with **23**.TNB or **23**.TNT regenerated the initial supramolecular oligomeric structure. The formation of donor–acceptor complexes between molecular ''clips'' (**23–24**) and NACs were rationalized and evidenced by single crystal X-ray diffraction analysis, ^{1}H NMR titration and significant changes in photoluminescence characteristics. Receptor **23** showed characteristic pyrene monomer emission along with a broad excimer emission at a longer wavelength (λ = 470 nm) in dilute $CHCl_3$ solution, which implied that two-pyrenyl moieties interact each other. However, receptor **24** displayed only the pyrene monomer emissions (λ = 375 and 400 nm), which reflected the absence of intramolecular π–π interactions. The emission intensities of molecular ''clip'' receptors were quenched effectively upon gradually increasing the concentration of TNB and TNT in chloroform and these changes were accompanied by sharp visual color changes from colorless to red for **23** or orange for **24**. The estimated binding constants from ^{1}H NMR titrations were $7.32 \times 10^4\ \mathrm{M}^{-1}$ **23**.TNB and $7.69 \times 10^2\ \mathrm{M}^{-1}$ for **23**.TNT. Exposure to several other NACs also found to form similar donor–acceptor complexes with receptors **23** and **24**.[36]

In 2010, Sessler *et al.* developed an effective fluorescent sensor dipyrenylamidocalix[4]arene-[15]crown-5 (**25**) that underwent analyte induced fluorescence quenching in the presence of NACs both in solution and solid-state.[37] The pyrenyl fluorophores were appended to the core calix[4]arene unit through amide linkage and the presence of polyether bridging on the core calyx[4]arene unit brought the two pyrene substituents parallel to the cleft of the incoming NACs. Sensor **25** displayed typical pyrene monomer (λ = 375 nm) and excimer (λ = 470 nm) emission upon excitation at 343 nm in acetonitrile solution. These emission bands were depleted in the presence of TNT or TNB even down to the ≈1.1 ppb level and sharp color change from colorless to red or orange for **25**.TNT and **25**.TNB, respectively. However, the addition of electron-neutral and electron-rich aromatics such as toluene, benzoic acid, ethyl benzoate, benzonitrile and phenylthiocyanate caused little or no quenching. The interaction between **25** and TNT was proved by single crystal X-ray diffraction analysis which revealed that two pyrene groups are oriented in an equatorial conformation to the core calix[4]arene unit and bind outside of the putative cleft with co-crystallized TNT molecules at a distance of 3.2–3.6 Å.[37]

3. Anthracene based sensors

Due to the π-electron-richness, high chemical stability, and strong photoluminescence characteristics, anthracene and its derivatives have been used extensively as fluorescence probes

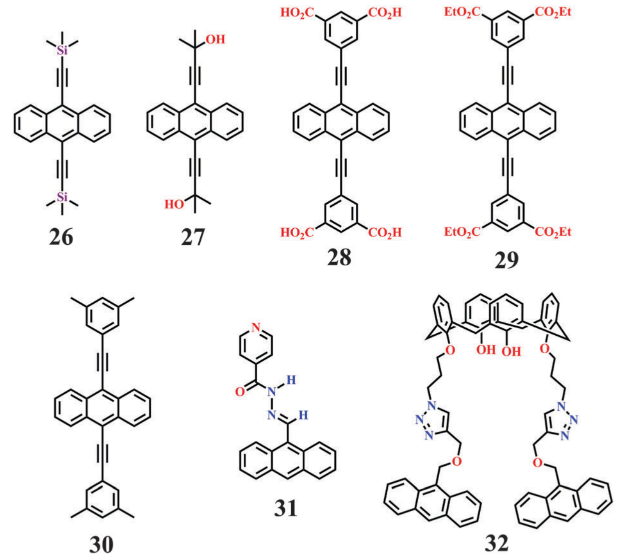

Chart 5 Electron rich fluorescence sensors containing the anthracene backbone.

for explosive detection (Chart 5). Recently, Mukherjee and co-workers designed π-electron-rich anthracene based fluorophore **26** bearing trimethylsilylethynyl (TMS) groups.[26] The attachment of bulky-TMS groups on the periphery of the anthracene-core further increases the conjugation through interactions between C–Si σ bonds and C≡C π bonds and also prevents the self-quenching of the fluorophore. The intense emission of **26** in $CHCl_3$ solution quenched efficiently upon addition of nitroaromatics such as TNT and PA at as low as ppb concentration; whereas, the addition of electron-deficient non-nitroaromatics such as BQ, BA *etc.* showed poor quenching responses even at higher concentration. The calculated Stern–Volmer binding constants (K_{SV}) were 1.97×10^4 M^{-1} for TNT and 2.15×10^5 M^{-1} for PA. The observed higher fluorescence quenching responses of NACs for **26** surmised to the strong dipolar or electro-static interactions between electron-rich fluorophore **26** and electron-deficient NACs *via* charge-transfer complex formation. In addition, the vapor-phase fluorescence study of the freshly made thin film of **26** showed significant quenching of emission intensity upon exposure to the saturated vapors of 4-NT. Nearly 40% quenching was observed after 7 min exposure of the film of **26** to 4-NT vapors. Notably, the fluorescence quenching responses of the thin film of **26** for PA was highly reversible.[26]

In 2013, the same group synthesized a similar anthracene based compound **27** incorporating bulky 2-methyl-3-butyn-2-ol $[HO\text{-}C(CH_3)_2]$ groups, which helped the sensor to self-associate into an infinite supramolecular polymeric network *via* intermolecular hydrogen bonding (O···HO) interactions and also avoided self-quenching of the adjacent discrete fluorophore unit.[27] The initial high fluorescence emission of **27** in $CHCl_3$ solution depleted rapidly upon addition of TNT and 2,4-DNT at ppb concentrations (2.0 ppb for TNT and 13.7 ppb for 2,4-DNT) and calculated quenching constants (K_{SV}) were 8.7×10^4 M^{-1} for TNT and 8.5×10^4 M^{-1} for 2,4-DNT. The decrease in the HOMO–LUMO energy difference of sensor **27** after binding with 2,4-DNT indicated a strong charge-transfer complexation and thus efficient fluorescence quenching (Fig. 5).

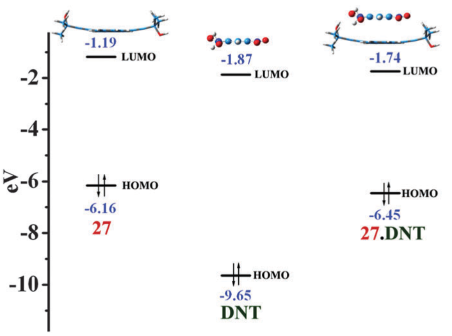

Fig. 5 Frontier orbital energy correlation diagram of sensor **27**, DNT and their complex **27**.DNT. Adapted with permission from ref. 27. Copyright 2013 Royal Society of Chemistry.

Interestingly, compound **27** showed differential and selective quenching responses for NACs over other interfering aromatic compounds such as toluene, chlorobenzene (ClB), BQ and maleic anhydride (MA). The vapor-phase quenching study of **27** implied that the sensing process was reversible and efficient for NACs. The freshly made thin film of **27** exhibited nearly 50% reduction in initial intensity after 360 s exposure to saturated vapor of 2,4-DNT. The high quenching efficiency of **27** in a short exposure time is attributed to the rapid diffusion of excitons along the supramolecular polymeric chain in the solid-state and this can be understand from single crystal X-ray diffraction analysis. Compound **27** adopted 2D supramolecular layers *via* H-bonding (1.97 Å) in solid-state, which further extended to a compact 3D network *via* π–π interactions (3.35 Å).[27]

In another contribution, Mukherjee *et al.* reported 3,5-bis(carboxyphenyl)ethynyl-substituted anthracene compound **28.**[38] The X-ray structural analysis revealed that 9 and 10-positions of anthracene are connected to two 5-ethynylisophthalic acids; and –COOH groups of each 5-ethynylisophthalic acid moiety is involved in intermolecular hydrogen bonding with neighboring molecules to form an infinite 1D supramolecular chain (Fig. 6). Two analogous compounds **29** and **30** were also synthesized by replacing –COOH in **28** with –COOEt (**29**) and CH_3 (**30**) to substantiate the role of H-bonding interaction in sensitivity of detection. Unlike **28**, molecular structure analysis of **29** revealed that it does not form such a supramolecular polymeric structure due to the lack of required H-bonding interactions. Compounds **28–30** exhibited strong emission in solution with estimated quantum yields of Φ = 0.21 (**28**); 0.23 (**29**) and 0.47 (**30**). The fluorescence quenching titration study of **28–30** with picric acid demonstrated that, as expected, the quenching efficiency followed the order **28** > **29** > **30**. The calculated quenching constants (K_{SV}) were 2100 M^{-1} (**28**); 200 M^{-1} (**29**) and 130 M^{-1} (**30**). In addition, a similar titration study with a series of analytes indicated the largest quenching responses of **28–30** for NACs at the ppb level over other analytes BQ and BA, which were elicited poor fluorescence quenching. Moreover, the emission intensity of the film of **28** decreased rapidly upon exposed

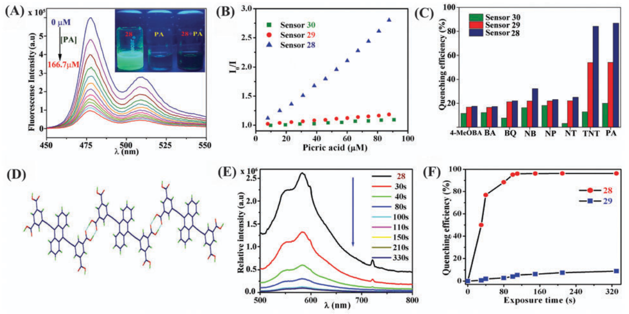

Fig. 6 (A) Reduction in the emission intensity of **28** upon gradual addition of PA (inset: visual color change of **28** before and after titrating with PA under UV-light). (B) Corresponding Stern–Volmer plots for the titration of **28–30** with PA at room temperature. (C) A plot of observed quenching efficiency for **28–30** upon the addition of different analytes. (D) A solid-state packing diagram of **28** exhibiting a pair-wise infinite 1D-supramolecular polymeric chain. (E) Time dependent emission intensity of the thin film of **28** upon exposure to the saturated vapour of NB and observed quenching efficiency of **28** and **29** as a function of the exposure time (F). Adapted with permission from ref. 38. Copyright 2011 Royal Society of Chemistry.

to NB vapor at room temperature. The quenching was about 77% upon 35 s exposure and increased to 96% after just 110 s exposure; this was very high compared to **29** (∼8% quenching observed after 300 s exposures). Notably, the thin film of **28** also showed highly reversible sensing towards NACs and the efficient quenching responses of **28** surmised to the formation of a supramolecular polymeric structure and also due to the easy passage of analytes into the intrinsic internal porosity. Thus it confirmed that, indeed, supramolecular H-bonding interaction influenced the dramatic change in sensitivity/efficiency of the sensor in the solid state (Fig. 6).[38]

In 2011, Wang *et al.* reported a *N*-acylhydrazone-anthracene based receptor **31**, which was synthesized by condensation of isonicotinohydrazide with anthracene-9-carbaldehyde in CH_3OH. This compound has multiple hydrogen-bond and π–π interaction sites for the specific recognition of PA.[39] The strong excimer emission of **31** at λ = 483 nm was quenched prominently along with a sharp visual color change from pale yellow to deep yellow upon the addition of PA solution. The initial intensity decreased to 3% when 3.0 equivalents of PA were added. Among various NACs titrated with **31**, only PA showed significant quenching, while other NACs such as TNT, DNT, NB, NP, 1,3-dinitrobenzene (DNB), 4-nitrobenzoic acid (NBA) and nitramine (RDX, HMX) caused poor quenching of intensity. The high selectivity of **31** for PA was, univocally, confirmed by single-crystal X-ray diffraction analysis, which revealed that the formation of a 1 : 1 complex between **31** and PA. The –N atom on the pyridine group was protonated to form a cation, while PA was deprotonated to form the anion, which can be further self-assembled to form a supramolecular network through multiple H-bonding and π–π interactions.[39]

In 2013, Zhang *et al.* synthesized a sensitive anthryl calix[4]arene based compound **32** with two anthracene fluorophores linked to the lower rim of calix[4]arene by a bridging triazole-linker and evaluated its sensing properties towards NACs.[40] Compound **32** showed three characteristics emission bands due to anthracene at 390 nm, 411 nm and 436 nm and the intensity of these bands diminished after the addition of NACs. Among them, PA caused significant quenching (97%), but the other NACs were found to be insensitive. The association constant (K_a) of **32** for PA was found to be 3.75×10^4 M^{-1} and Job's plot analysis indicated a 1 : 1 complexation. Furthermore, the computational modeling disclosed that PA was sandwiched in between two anthryl fluorophores by π–π stacking (d = 4.1 Å).

4. Carbazole based sensors

Carbazole is a tricyclic heteroaromatic compound having two benzene rings fused on both sides of the pyrrole unit. It has been found to have a wide range of applications in optoelectronics in recent years.[41] The π-electron richness and interesting photo/electroluminescent properties of carbazole and its derivatives have made them efficient chemosensors for NAC detection (Chart 6). Recently, the nitroaromatic sensing nature of fluorescent quino[2,3-*b*]carbazole derivative (**33**) has been demonstrated.[42] **33** displayed a bright green emission at λ = 530 nm in $CHCl_3$ and strong red-emission at λ = 626 nm in solid-state. This intense emission was attributed to the lack of intra/intermolecular hydrogen-bonding interactions in solution and to the lack of effective π–π stacking interactions in the solid-state. The bright emission of **33** attenuated upon the incremental addition of NACs (10 μM in CH_3CN) such as NB, TNT, 2,6-DNT, 1,3-dinitrobenzene (1,3-DNB) and 1-chloro-2,4-dinitrobenzene (Cl-2,4-DNB). The binding between **33** and

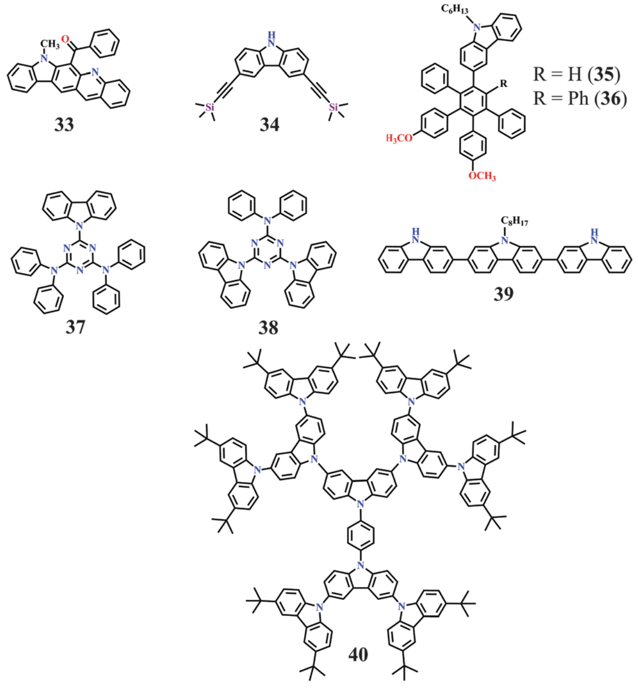

Chart 6 Examples of a few small molecule sensors containing the carbazole backbone.

NACs was also inferred from the clear visual color changes and the observed fluorescence quenching. The authors described such quenching due to the π donor–acceptor (D–A) complex formation.

Mukherjee *et al.* synthesized a novel 3,6-carbazole functionalized fluorescence sensor **34** by incorporating trimethylsilylethynyl substituents *via* a Sonogashira coupling reaction between 3,6-dibromocarbazole and trimethylsilylacetylene.[26] The fluorescence emission of **34** was shifted to a longer wavelength compared to its starting precursor 3,6-dibromocarbazole, due to strong σ–π interactions between C–Si σ bonds and C≡C π bonds. Compound **34** emits at λ = 375 nm with a calculated fluorescence quantum yield of Φ = 0.078 and the initial emission intensity was quenched efficiently and displayed a differential fluorescence quenching among various NACs, which helped to discriminate the structurally related nitroaromatic explosives. Notably, a similar fluorescence titration with other electron-deficient analytes such as BQ, 4-methoxy-benzoic acid (4-MeOBA), BA elicited poor fluorescence quenching due to their weak binding with **34**.

Kumar *et al.* synthesized aggregation induced emission enhanced (AIEE)-active hetero-oligophenylene carbazole derivatives **35–36** and explained their binding properties towards various nitroaromatic compounds, *viz.*, TNT, 2,4-DNT, PA, 4-NB, 4-NP, 2,3-dinitro-2,3-dimethyl butane (2,3-DN-2,3-DMB) and also two reference analytes such as BA and BQ.[43] The fluorescence emission spectrum of **35** exhibited weak emission in THF at 363 nm (Φ = 0.0018) and the emission was dramatically enhanced (Φ_{AIEE} = 0.59) upon addition of 80% volume fraction of H_2O. Similar emission characteristics were noticed for **36** (Φ_0 = 0.006, Φ_{AIEE} = 0.43). The observed emission enhancement in aqueous medium was attributed to the restricted intramolecular rotations by formation of self-aggregates. The AIEE emission of **35** and **36** decreased exhibiting a visual color change upon addition of TNT (10 μM for **35** and 13 μM for **36**). The estimated quenching efficiencies were 94% and 92%, respectively. The detection limits were found to be 30×10^{-9} (**35**) and 40×10^{-9} mol L^{-1} (**36**). However, only 40% fluorescence quenching was observed for **35** in pure THF in the presence of 10 μM TNT. The calculated quenching constants from the linear Stern–Volmer plots of **35** and **36** were 13.3×10^5 M^{-1} and 10.0×10^5 M^{-1} respectively, and the efficiency of fluorescence quenching for different NACs followed the order TNT > 2,4-DNT > PA > 1,4-DNB > 4-NT > NB > 4-NP. It is noteworthy to mention that no fluorescence quenching was observed upon addition of BA and BQ. The authors proposed that the observed fluorescence quenching of aggregates of **35** and **36** in the presence of NACs was ascribed to the static quenching *via* a charge transfer complex. It was also described the quenching propensity of **35** and **36** to the saturated vapors of TNT at room temperature. Exposure of the solution of **35** and **36** in 8 : 2 H_2O/THF to saturated vapors of TNT for 1 min caused nearly 25% and 22% fluorescence quenching, respectively, and the quenching increased to 80% and 85% respectively, after exposing for 30 minutes. In addition, the authors also demonstrated the sensing ability of **35** and **36** on Whatman-filter paper and glass-plates to the vapors of TNT.[43]

In 2012, Huang and co-workers designed two conjugated asymmetric donor–acceptor (CADA) fluorophores (**37** and **38**) framed with two-different donors of carbazole and diphenylamine that were connected to a core triazine acceptor unit.[44] Both fluorophores **37** and **38** displayed an unusual blue-shifted ultraviolet emission and narrow photo-luminescent spectra with dramatic enhancement in the fluorescence intensity in the solid-state than that in solutions, which inspired the authors to explore the aggregation-induced emission (AIE) behavior in mixed solvents. The emission spectra of **37** in THF/water mixtures increased (at 378 nm and 398 nm) dramatically as the water fraction increases. A nearly 670-fold enhancement in intensity was observed at 378 nm when the water fraction was 90%. A similar emission enhancement (at 373 nm and 393 nm) was noticed in the case of fluorophore **37** when the water fraction was increased. The emission spectrum at 393 nm was enhanced to 139-fold when the water fraction was 98%. The reason for the observed increased emission characteristics of **37** and **38** was the aggregation-induced behavior in the THF/water solvent mixture. Owing to their propeller-like shapes, extended π-conjugation and AIE behaviors, fluorophores **37** and **38** were used as sensors for PA. The emission intensity of aggregates of **37** and **38** was progressively attenuated with no change in the spectral profile even in the presence of as low as 15 ppb concentration of PA. No change in the fluorescence life-time of both the aggregates upon increasing the concentration of PA implied that the observed fluorescence quenching mainly followed the static mechanistic pathway and Stern–Volmer binding constants at low concentrations (<0.08 μM) of PA were 1.48×10^7 M^{-1} (**38**) and 1.69×10^7 M^{-1} (**37**). It is noteworthy to mention that the binding strength between **37** and **38** and PA becomes weaker when the titration was carried out in pure THF and the relevant quenching constants estimated were 2.50×10^6 M^{-1} (**38**) and 2.54×10^6 M^{-1} (**37**). The fluorescence quenching behaviors of **37** and **38** were highly selective for PA even in the presence of many other interfering common chemicals and other NACs.[44]

An organic fluorescent nanofibril was fabricated from a linear 2,7-linked carbazole trimer (**39**) and demonstrated to be an efficient and fast responsive fluorescent sensor for NACs such as TNT, DNT.[45] The carbazole-trimer **39** was made from 2,7-dibromo-9-octyl-9*H*-carbazole and 9*H*-carbazole-2-boronic acid pinacol ester in one step by Suzuki-coupling reaction. The introduction of the long-chain octyl group increased the solubility and facilitated the intermolecular arrangements of **39** to adopt a self-assembled fluorescent organic nanofibril.

The strong blue-emission of the nanofibril film at 438 nm was quenched efficiently when exposed to saturated vapors of DNT and TNT. Nearly 50% and 70% quenching efficiencies were observed after exposing the film to the saturated vapors of TNT for 30 and 60 s, respectively. The rate of fluorescence quenching was much faster (within 2.4 s) when the film was exposed to the saturated DNT vapor, for which 50% quenching was achieved in only 10 s and the observed fluorescence quenching was highly reversible. Rapid fluorescence quenching of these sensory materials was due to the photoinduced electron-transfer from the excited nanofibril of carbazole-trimer (**39**) to the surface adsorbed NACs. A similar fluorescence quenching was also noticed in steady-state fluorescence titration in solution. For instance, DNT binds with carbazole-trimer **39** in solution with an estimated binding constant of 720 M^{-1}. The easy tunable intrinsic porosity, large surface area and efficient fluorescence quenching implied the potential applications of the nanofibril of **39** as a sensory material for on-site NAC detection.[45]

A highly conjugated, propeller-shaped carbazole-based sensor (**40**) with *tert*-butyl surface groups displayed gelatin behavior was reported. This compound formed a three-dimensional porous network structure with the nanofibril entangling and intersecting each other.[41c,46] The xerogel film of **40**, due to the strong π-donation and intrinsic porosity, was used as a fluorescence sensor for monitoring the presence of NACs such as TNT and 2,4-DNT in vapor-phase. Exposure of the xerogel film of **40** to the saturated TNT and 2,4-DNT vapors caused nearly 77% and 91% quenching efficiencies, respectively. On the other hand, the amorphous form of **40** caused almost 51% for TNT and 77% for 2,4-DNT fluorescence quenching. The observed higher fluorescence quenching of the xerogel film was attributed to its porous nature, which allows the easy and fast diffusion of NACs compared to the as-spun amorphous film.

5. Fluoranthene based sensors

Fluoranthene and its derivatives have attracted increasing attention in recent years owing to their strong fluorescence with small Stoke's shifts and potential applications in organic-light emitting materials.[47] Accordingly, fluoranthene based materials were employed as fluorescence sensors for the detection of explosive debris (Chart 7). In 2012, Patil and co-workers reported two π-electron-rich fluoranthene based fluorescence sensors **41** and **42** for trace and selective detection of NACs at a ppb level of concentration (Chart 7).[48,49] Compound **41** was synthesized by Knoevenagel condensation between 1,3-bis(4-bromophenyl)propan-2-one and acenapthenedione,[48] while **42** was obtained by a three-step synthetic process employing 1,2-bis[4-(hydroxyl)phenyl]ethyne and 7,9-bis-(4-bromophenyl)-8*H*-cyclopenta[*a*]acenaphthylen-8-one in ethanol medium.[48,49] The presence of –Br atoms and the unsymmetrical phenyl moiety in **41** effectively helped the self-association *via* π–π interactions and formed 1D-supramolecular arrangement in solid-state through layer-by-layer self-assembly, while solid-state packing of **42** revealed a Z-shaped supramolecular arrangement stabilized by strong C–H···π interactions. The difference in structural arrangements and intrinsic micro-porosity envisaged that both **41** and **42** could be potential sensors that intercalate the electron-deficient NACs *via* π–π interactions and thus exert an efficient quenching propensity. The strong blue emission of **41** at 452 nm (with a Stoke's shift of 82 nm and a lifetime of ~8.079 ns) and at 475 nm for **42** (with a Stoke's shift of 101 nm and a lifetime of 11.37 ns) decreased significantly upon increasing the concentration of NACs such as PA, DNT and TNT. Almost 76% and 80% quenching in intensity of **41** and **42** was noticed in the presence of 10 μM and 0.1 mM concentration of PA, respectively. The estimated quenching constants (K_{SV}) from titration profiles were 9.9×10^4 M^{-1} for PA; 860 M^{-1} for DNT; 1609 M^{-1} for TNT with **41** and 1.24×10^5 M^{-1} for PA; 1772 M^{-1} for DNT; 1828 M^{-1} for TNT with **42**. The obtained linear SV plot and invariant fluorescence lifetime with the increasing concentration of PA suggested that the observed fluorescence quenching follows the static mechanism through ground-state donor–acceptor complex formation. Notably, a similar titration study with other electron-deficient analytes showed little effect on initial intensity, whereas NACs engendered significant quenching with a detection limit of 2–20 ppb for PA, while DNT and TNT showed a 1.1 ppb/ppm level of detection.[48] The initial emission intensity of the freshly made thin film of **41** quenched almost 80% upon 600 s exposure to saturated vapor of PA, while **42** exhibited 92% quenching after 420 s exposure. The observed vapor-phase quenching was recovered after several cycles of exposure, which implied that both **41** and **42** can be potential sensor materials for NAC sensing.

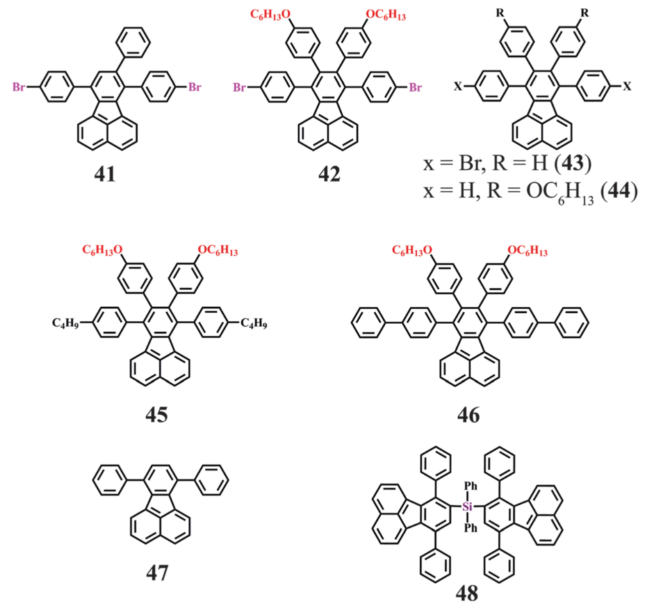

Chart 7 A series of fluoranthene based sensors.

In continuation, the same group in 2013 demonstrated the sensing of a series of fluoranthene derivatives. These were synthesized *via* Diels–Alder reactions followed by decarbonylation by varying the substituents (–Br, $-C_6H_{13}$ and phenyl moiety) on the fluoranthene moiety.[50] The presence of alkoxy ($-C_6H_{13}$) chains on phenyl rings in **44–46** enhanced the solubility in common solvents and induced the enough flexibility to show unique supramolecular arrangements in solid-state. Attachment of bulky phenyl moieties on the surface of fluoranthene core prevents the self-aggregations *via* π–π interactions and maintains their photostability. The solid-state structure of **44** is stabilized by strong C–H···π (2.88 Å) interactions between alkylated C–H and π-clouds of phenyl moieties and also by

O···H (2.685 Å) interactions to form a unique supramolecular network. On the other hand, solid-state structure of **45** is stabilized by two kinds of C–H···π (2.609 Å) interactions involving alkylated C–H and phenyl rings and another C–H···π (2.81 Å) between two phenyls rings to adopt an interesting humanoid-like supramolecular arrangement. All the fluoranthene derivatives showed strong blue-emission at ~475 nm with a Stoke's shift of 103 ± 2 nm. Compound **44** exhibited relatively less emission intensity due to the heavy atom effect of the -Br atom. All these sensors exhibited the quantum yield in the range 26–34% and the fluorescence lifetime was found to be in the range 8.23–11.87 ns. The strong blue emission intensity of all these sensors at ~475 nm in solution (1 μM) was attenuated gradually upon increasing the concentration of NACs. Sensor **46** showed almost 90% quenching in the presence of 10 μM of PA with a quenching constant K_{SV} = 2.405 × 10^5 M^{-1}. Among different NACs, PA displayed the highest quenching response as low as 2–20 ppb, while DNT and TNT exhibited ~1.1 ppm level of detection. The calculated quenching constants of the sensors with PA follow the order **46** > **45** > **44** > **43.** Notably, no such pronounced quenching was observed upon addition of other electron-deficient non-nitroaromatics implying the high selectivity of these sensors for NACs. Furthermore, the initial emission intensity of the thin films gradually decreased as a function of the exposure time to saturated vapors of NACs. The vapor-phase high sensitivity towards 60 s exposure to PA vapor follows the order **46** > **45** > **44** > **43**. The authors also demonstrated the sensing performance of thin films in water containing low concentrations of PA (50 μmol L^{-1}) and the quenching rate constants were found to be 1.58 × 10^4, 2.67 × 10^4, 5.49 × 10^4 and 7.96 × 10^4 for **43**, **44**, **45**, and **46**, respectively. Moreover, a femtogram detection level ~1.15 fg cm^{-2} was noticed for PA and TNT by the contact mode approach on thin layer silica chromatographic plates.[50]

Xie *et al.* have designed and synthesized two fluoranthene-based sensors: nonsilicon-cored 7,10-diphenyl-fluoranthene (**47**) and silicon-cored bis(7,10-diphenyl-fluoranthene)diphenylsilane (**48**) starting from acenaphthenequinone and 1,3-diphenylpropane-2-one.[51] Compared to **47**, compound **48** showed stronger emissions both in solution as well as a thin-film because of its tetrahedral structure that could effectively prevent intermolecular aggregation *via* π–π interactions. The strong emission of both **47** (446 nm in THF) and **48** (453 nm in THF) was quenched efficiently both in solution as well as a thin-film upon addition/exposure to nitrobenzene and m-dinitrobenzene. Nearly 71% and 80% quenching efficiencies were observed for **47** and **48,** respectively, when the NB concentration was ~1500 ppm. The addition of DNT (500 ppm) caused 58% and 68% fluorescence quenching of **47** and **48**, respectively. Notably, the sensors indicated the presence of NB as low as 100 ppm (**47**) and 50 ppm (**48**). Moreover, the emission intensity of **48** was quenched completely after 120 s exposure to NB vapor, while the film of **47** displayed complete fluorescence quenching after 180 s exposure. The observed higher quenching efficiency of **48** can be ascribed to its "V" shaped non-coplanar tetrahedral structure that complicates its aggregation and enhanced the π–π interactions between **48** and NACs. The planar structure of **47** allowed the easy aggregation *via* self-association resulting in weak binding affinity and in turn, caused less fluorescence quenching.[51]

6. Pentiptycene based sensors

The pioneering work of Swager *et al.* on iptycene based conjugate polymer sensors, which were commercialized as Fido® portable devices for NAC detection has inspired many research groups to design novel sensors with improved sensitivity.[52] Very recently, Anzenbacher and co-workers have designed a series of 1,4-diaryl pentiptycene-based small molecule sensors (**49–54**) for efficient detection of NACs both in solution and vapor phase (Chart 8).[53,54] In comparison to other planar PAHs, iptycene-based sensors provide an electron-rich open cavity due to their 3D molecular structure, which is capable of binding electron-deficient NACs in an edge-to-face mode, rather than the very common donor–acceptor stacking interactions.

The sensors **49–54** were synthesized from 1,4-dichloro- or 1,4-difluoro-2,5-diarylbenzene derivatives by double base-promoted dehydrohalogenation to give corresponding arynes, which upon further cycloaddition with anthracene yielded 1,4-diarylpentiptycenes.[53] The steric crowding and the iptycene bridgehead H-atoms constrained the fluorogenic aryl fragments, attached at the 1 and 4-positions of the central benzene ring to assume a perfect perpendicular orientation with respect to the central benzene ring. Such reduction in π-conjugation increased the HOMO–LUMO band gap in **49–53** and hence enhanced the efficiency of electron-transfer to NACs. Compounds **49–53** showed strong photoluminescence characteristics with relatively modest quantum yields (Φ_F = 0.10–0.20) due to their poor electronic conjugations and also due to the presence of sulfur atoms. As expected, the initial emission intensity of **49–53** was quenched dramatically upon increasing the concentration of NACs. For instance, fluorimetric titration of **50** with TNT elicited significant quenching at 345 nm and displayed a non-linear Stern–Volmer plot that implied the mechanism of quenching follows both static and dynamic pathways. The binding constant (K_{SV}) calculated from the initial part of the plot (low concentration region) was 3.3 × 10^3 M^{-1}. Similar titrations of all these sensors with different NACs (NB, 2,4-DNT, TNT) showed a similar effective quenching phenomenon and the estimated quenching

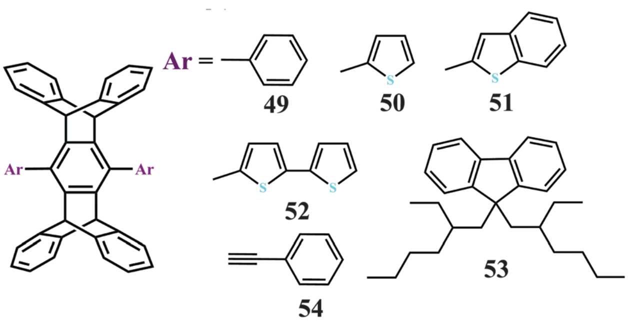

Chart 8 Pentiptycene-based small molecule sensors.

constants followed the order NB > 2,4-DNT > TNT. The observed higher quenching efficiency of NB with **49–53** was ascribed to the perfect fitting of NB within the iptycene cleft, whereas TNT and 2,4-DNT showed moderate quenching effects owing to their larger molecular sizes that did not fit well with the cleft. Conversely, compound **54** showed poor quenching than **49–53** because of the high degree of conjugation with the central iptycene moiety that lowered the LUMO energy and reduced the efficiency of electron-transfer to NACs.[54] Finally, the mode of binding was, unambiguously, proved by X-ray diffraction analysis of the **51**and NB host–guest complex. The diffraction analysis revealed that two benzothiophene units are perpendicular to the central benzene ring of iptycene with a dihedral angle of 81.98 Å and the NB molecule fits perfectly within the iptycene cleft in an edge-to-face binding mode. Moreover, the solution-cast polyurethane thin films of **49–53** showed similar quenching patterns in the solid-state after exposing the films to saturated vapors of NACs.[53,54]

7. Triphenylene based sensors

Among the family of PAHs, triphenylene and its derivatives (Chart 9) are expected to be superior fluorescence sensors for explosive detection owing to their symmetrical planar structure and extended π-conjugations tend to form strong donor–acceptor complexes with electron-deficient NACs.[55] The vacuum sublimation of monomeric triphenylene (**55**) formed 1D micro/nano crystalline fluorescence fibers, engendered detectable fluorescence quenching upon exposure to saturated NB vapor, while the saturated vapors of benzene, methanol, methylformate, acetone and nitromethane caused no quenching due to the lack of electron-withdrawing $-NO_2$ groups and aromatic rings.[56] Despite detectable binding with NACs, the sensitivity of monomeric triphenylene is less due to the low luminescent quantum efficiency. However, the quenching sensitivity can be improved by introducing suitable functional groups on the core triphenylene unit.

Accordingly, Bhalla *et al.* synthesized triphenylene derivative **56**, decorated with carbazole groups on the periphery following a Suzuki–Miyaura coupling of 9-hexyl-9*H*-carbazole-3-ylboronic acid and 2,3,6,7,10,11-hexabromotriphenylene.[57] The presence of bulky carbazole moieties increased the π-conjugation and also prevents the possible intermolecular π–π stacking aggregation. The intense emission at 410 nm (Φ = 0.50) of **56** was completely quenched in the presence of PA (50 equiv.) including a clear color change in mixed aqueous medium. The calculated K_{SV} was 2.91 × 10^5 M^{-1} and the detection limit was found to be 400 nm. Notably, the addition of various other NACs such as 4-NT (85 equiv.), DNB (200 equiv.), DNT (260 equiv.) and TNT (300 equiv.) also induced the complete quenching of emission, while the addition of other electron-deficient aromatics such as BQ (1500 equiv.) caused very poor quenching effects. The authors also demonstrated the contact-mode detection of PA as low as 14 pg cm^{-2} using a test strip coated with a THF solution of **56**.[57] The same group, in another contribution, described the NAC sensing ability of two triazole-modified triphenylene fluorescence sensors **57** and **58**. These compounds formed supramolecular aggregates based on π–π interactions, dipole–dipole and van der Waals interactions, both in bulk and solution phases.[58] Sensors **57** and **58** formed emissive and thermoreversible organogels in cyclohexane and a mixture of solvents, such as hexane and dichloromethane (1 : 4, v/v). The high emission of **57** at 383 nm (Φ = 0.31) with two shoulder bands at 371 and 403 nm was quenched completely upon the addition of PA (270 equiv.) in DMSO, whereas, **58** showed emission at 384 nm, which was quenched fully upon addition of 30 equiv. of PA with a detection limit of 50 nM and a calculated binding constant of K_{SV} = 2.93 × 10^5 M^{-1}. Similar quenching propensities were also realized upon addition of other NACs in much higher concentration for both the compounds **57** and **58**. Furthermore, the dip-coated organogels onto the TLC strips exhibited rapid fluorescence quenching upon exposure to NACs.[58]

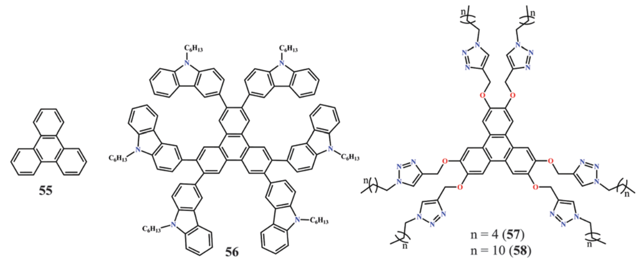

Chart 9 Triphenylene based sensors for NACs.

8. Triphenylamine based sensors

The free rotatable C–N single bonds and non-planar nature helps triphenylamine derivatives to form unique supramolecular organic electronic materials.[59] The aggregation-induced emission, in particular, provides large internal voids for the exciton to migrate. Very recently, Molina *et al.* have synthesized a novel triphenylamine-based sensor **59** substituted with imidazo-benothiadiazole moiety and used it to selectively sense NACs, with discriminating ability between phenolic- and non-phenolic NACs (Chart 10).[60] Compound **59** was obtained in high yield by condensation between 4,5-diamino-2,1,3-benzothiadiazole and 4-diphenylaminobenzaldehyde and displayed an intense emission at 488 nm in toluene to 595 nm in DMSO with a large Stoke's shift. The initial emission intensity of **59** died down rapidly upon addition of NACs. Significant quenching efficiency was observed for phenolic-NACs (4-NP and PA), while NB showed poor quenching and moderate quenching was noticed for 2,4-DNT, 2-nitrotoluene (2-NT) and 2,4-DNB. The analysis of the emission titration profile implied that **59** formed a 1 : 1 complex with PA and the calculated binding constant was K_a = 4.49 × 10^3 M^{-1}. According to the ^1H NMR titration study, it was concluded that the presence of the –OH group in phenolic-NACs involved in hydrogen-bonding interactions with the N-atoms of **59** along with strong π–π stacking with the triphenylamine fluorophore,

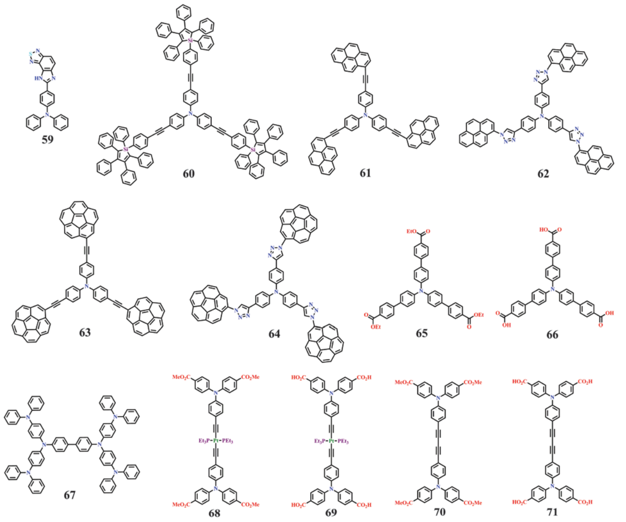

Chart 10 Triphenylamine functionalized molecular sensors.

which in turn displayed a discriminating sensing behavior between phenolic and non-phenolic NACs.[60]

In 2011, Zhao and co-workers designed and synthesized a starburst fluorescence sensor **60** containing triphenylamine decorated on the periphery with multiple 1,1,2,3,4,5-hexaphenylsiloles *via* Sonogashira coupling reaction.[61] The siloles groups were attached to triphenylamine owing to their unique electronic properties and aggregation-induced emission characteristics. The starburst 3D conformation of **60**, due to a "propeller-like" shape of peripheral attached siloles, is expected to hamper the intermolecular stacking interactions and creates void space for easy access of explosive analytes. The addition of a large amount of water fraction to the non-emissive THF solution (10 mM) of **60** induced the intense emission at 495 nm and this was quenched upon PA addition even at the level of 1 ppm. Virtually no emission was observed in the presence of 78.5 mM concentration of PA with an estimated binding constant of $K_a = \sim 7 \times 10^4$ L mol^{-1}. The observed fluorescence quenching was probably due to the energy transfer from the excited state of **60** to the ground state of PA. Moreover, the intense greenish blue emission of a filter paper strip coated with **60** faded after dropping PA solution on it.[61]

In 2012, Sukwattanasinitt and co-workers designed a series of triskelion-shaped triphenylamine based fluorescence sensors (**61–62**) containing pyrene and corannulene (**63–64**) fluorophores.[62] The acetylene-linked compounds (**61–62**) were synthesized from 4,4′,4″-triiodotriphenylamine *via* a Sonogashira cross coupling reaction with ethynyl pyrene and ethynyl corannulene; while triazole linked sensors (**63** and **64**) were obtained *via* a click reaction between 4,4′,4″-triiodotriphenylamine and 1-azidopyrene and 1-azidocorannulene. Upon excitation, **61** and **62** emitted at 484 and 494 nm, respectively, while **63** and **64** emitted in the lower energy region at 506 and 537 nm with large Stoke's shifts (∼200 nm) in all cases. The initial intense emission of **61–64** was attenuated in the presence of various quantities of TNT. The observed higher quenching efficiencies ($K_{SV} = 1.7 \times 10^4$ M^{-1} and 6.4×10^3 M^{-1}) of **63** and **64** compared **61** and **62** ($K_{SV} = 8.4 \times 10^2$ M^{-1} and 7.2×10^2 M^{-1}) suggested that triazole-linked sensors bind much strongly with NACs. The ^{1}H NMR titration study of **63** with TNT suggested that the $-NO_2$ group of TNT interacts with triazole-H and pyrene units bind with TNT *via* π–π interactions and also supported that observed quenching follows dynamic quenching pathways. Notably, the corannulene functionalized sensors **62** and **64** showed slightly lower quenching efficiencies due to the bowl shape geometry of corannulene compared to pyrene-functionalized **61** and **63** owing to the planar aromatic surface of the last pair. Furthermore, the contact-mode fluorescence sensing of **63** on top of a filter paper allowed visual detection of TNT at 0.58 ng mm^{-2} levels.[62]

Triphenylamine-based sensors (**65–66**) were synthesized and employed as superior chemosensors for trace detection of NACs.[63] Both **65** and **66** showed strong blue emission in THF solution at 455 and 450 nm with Stoke's shifts of 85 and 80 nm, respectively. The calculated quantum yields of **65** and **66** were 6% and 18%, respectively. The concentration-dependent emission studies in THF revealed that the observed emissions of **65** and **66** are due to aggregation-induced emission. The initial intensity was quenched selectively upon increasing the amount of PA solution including a sharp color change from colorless to intense yellow. The quenching efficiencies of **65** and **66** were found to be 82% (**65**) and 95% (**66**) and the detection limits were 40 ppb for **65** and 5 ppb for **66**. The Stern–Volmer binding constants (K_{SV}) in lower concentrations of PA were 2.98×10^6 M^{-1} (**65**) and 1.43×10^6 M^{-1} (**66**). The fluorescence titration studies and SEM analysis in combination with ^{1}H NMR titration studies suggested that the observed fluorescence quenching followed the static mechanism *via* ground-state complex formation possibly through multiple H-bonding interactions in solution. In addition, paper strips coated with compounds **65** and **66** served as simple and low-cost contact mode sensors for PA at an attogram level and also exhibited very selective quenching behaviors in vapor phase.[63] Zade and co-workers reported an extended π-conjugated triphenylamine-based dumbbell shaped sensor **67** for NACs.[64] Compound **67** displayed a strong blue emission at 446 nm with a quantum efficiency of 0.78 in benzene solution. The initial blue emission of **67** was quenched upon addition of different NACs. Only PA elicited a superior efficiency of 98% in the presence of 30 equivalents of PA and the detection limit was found to be 433 ppb. A linear Stern–Volmer plot with respect to the concentration of PA implied that quenching followed static mechanism with a quenching constant $K_{SV} = 1.82 \times 10^5$ M^{-1}. Interestingly, a paper strip coated with **67** showed drastic quenching after immersing into the aqueous solution of PA.

Very recently, Mukherjee *et al.* demonstrated the binding propensity of four triphenylamine based fluorophores **68–71** towards various NACs both in solution as well as in vapour phase.[65] The strong fluorescence emission of **68–71** in the range 420–460 nm was quenched rapidly upon mixing with NACs. Among them, **69** and **71** showed the highest quenching efficiency towards phenolic-NACs (PA, 2,4-DNP) compared to their corresponding ester analogues (**68** and **70**). The calculated binding constants were 5.72 × 10^6 M^{-1} (**69**); 2.9 × 10^5 M^{-1} (**71**) and the estimated detection limit was ∼5 ppb. Interestingly, compounds with carboxylic acid groups (**69** and **71**) showed a better fluorescence quenching response upon exposure to the NB vapors. Upon 50 s exposure of the freshly made thin film of **69** caused 80% fluorescence quenching, whereas **68** showed only 16% quenching. The observed superior fluorescence quenching responses of **69** and **71** compared to **68** and **70** were ascribed to the long-exciton migration through intermolecular interaction along the molecular backbone.

9. Triphenylbenzene based sensors

Triphenylbenzene is a π-conjugated, easily synthesizable and inexpensive C_3-symmetric class of fluorophores with a non-planar propeller-shape. Over the past decades, triphenylbenzene and its derivatives have been widely employed as molecular building units in the design of various porous materials (conjugated covalent polymer/metal–organic frameworks).[66] Very recently, Murugavel and co-workers synthesized an amino-substituted triphenylbenzene supramolecular fluorophore [**72**; 1,3,5-tris(4′-aminophenyl)benzene] that can selectively sense nitroaromatic explosives through donor–acceptor complexation.[67] In the solid-state, fluorophore **72** is interconnected *via* intermolecular hydrogen-bonding interactions between $-NH_2$ groups to adopt a three-dimensional supramolecular framework which is capable of encapsulating NAC analytes. The presence of $-NH_2$ groups further increased the binding propensity of **72** through intermolecular hydrogen bonding interactions with $-NO_2$ groups of NACs. The strong fluorescence emission of **72** at 405 nm in CH_3CN decreased in intensity (67–85%) with the increasing concentration of NACs such as PA, TNT, 2,4-DNT and 1,3-DNB. PA displayed a stronger binding affinity (K_{SV} = 1.2 × 10^5 M^{-1}) and also the highest fluorescence quenching (85%) owing to its high electron-deficiency coupled with facile proton transfer from acidic –OH of PA to the $-NH_2$ group of **72**. The estimated binding constants for other NACs were 4.0 × 10^3 M^{-1} (TNT), 8.3 × 10^3 M^{-1} (2,4-DNT), 2.6 × 10^3 M^{-1} (1,3-DNB). No change in the initial life-time (6.3 ns at 405 nm) of **72** with the increasing amount of PA indicated that fluorescence quenching followed the static mechanism. Similar fluorescence titrations with other interfering electron-deficient analytes such as hexafluorobenzene (HFB), 1,2,4,5-tetrafluorobenzene (TFB), benzonitrile (BCN) and chlorobenzene caused no quenching in the emission intensity. In addition, the emission intensity of the freshly made film dropped almost 60% upon 20 min exposure to vapors of NACs. The donor–acceptor complexation of **72** with NACs was unequivocally confirmed from the molecular structure analysis *via* co-crystallization. The X-ray diffraction analyses revealed that fluorophore **72** adopted vertically overlapped – donor–acceptor–donor–acceptor – types of π-stacking through strong intermolecular hydrogen bonding with electron-deficient NACs. PA and TNT bind in a 1 : 1 molar ratio with the central benzene unit of **72**, while 1,3-DNB formed 1 : 3 stoichiometric complexes through stacking between peripheral phenyl rings. The donor–acceptor adduct was further stabilized by hydrogen bonding between $-$the NH_2 group of **72** and $-NO_2$ groups of NACs (Fig. 7). To rationalize the role of hydrogen-bonding of the $-NH_2$ group in the quenching efficiency, the same group designed a discrete fluorophore [**73**; 1,3,5-tris(4′-(*N*,*N*-dimethylamino)phenyl)benzene] by replacing N–H protons with $-CH_3$ groups.[68] Unlike **72**, discrete sensor **73** selectively recognized PA (K_{SV} = 3.87 × 10^5 M^{-1}) even as low as 1.5 ppm, over other NACs such as TNT, 2,4-DNT, 1,3-DNB. Nearly 90% quenching efficiency was obtained for **73** in the presence of 16 equiv. of PA, while sensor **72** required almost 32 equiv. of PA to reach 90% quenching. The high selectivity of **73** compared to its parent sensor **72** towards PA was attributed to the enhanced basicity of $-NMe_2$ that abstracts protons from PA and forms N–H···O hydrogen bonding. This was further proved by X-ray diffraction analysis, which indicated the formation of a 1 : 3 complex between **73** and PA.[68b]

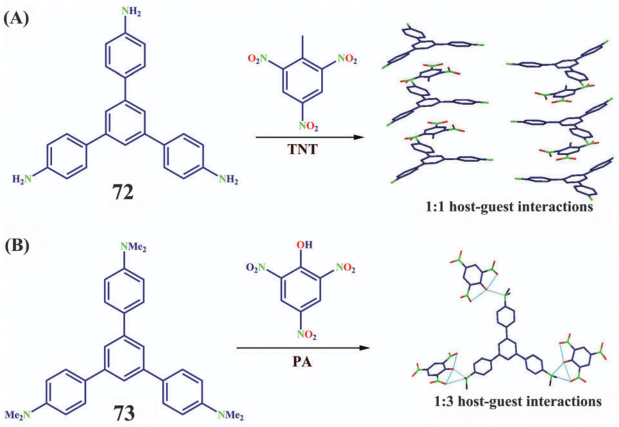

Fig. 7 (A) Molecular structure of **72** and its 1 : 1 host–guest complexation with TNT in solid-state. (B) The molecular structure of **73** and its 1 : 3 host–guest complexation with PA in solid-state. Adapted with permission from ref. 67 and 68. Copyright 2013/2014 Royal Society of Chemistry.

10. Coronene based sensor

Coronene and its derivatives, due to their planar, highly rigid and discotic core unit, have attracted tremendous interest over the decades in the area of materials and supramolecular chemistry.[69] However, their potential as fluorescence sensors for the trace detection of analytes is being limited because of their aggregation-caused fluorescence quenching through facile π–π stacking interactions. One possible way to overcome this problem is to introduce sterically demanding functional groups which in turn, decreases the effective π–π stacking between adjacent coronene moieties. Accordingly, Bhalla and co-workers designed and synthesized hexa-*peri*-hexabenzocoronene based fluorophores **74** and **75** that possess bulky *tert*-butyl groups to prevent the self-quenching in solution (Chart 11).[70]

Further, these compounds were appended with phenyl-rotors to enable the aggregation-induced fluorescence enhancements and were used as highly sensitive sensors for PA. The targeted chemosensors **74** and **75** were obtained in high yields by simple Suzuki–Miyaura cross couplings and they were weakly emissive in

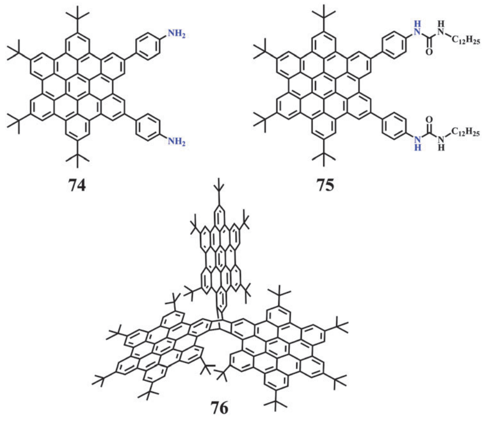

74 75 76

Chart 11 A few examples of coronene based molecular sensors for nitroaromatics.

pure THF solution. But the emission was enhanced to 67% for **74** (Φ_{AIEE} = 0.68) and 86% for **75** (Φ_{AIEE} = 0.73) by adding 40% of the H_2O content to the THF solution. The observed fluorescence enhancements were attributed to the freezing of phenyl group free-rotations in mixed aqueous medium. The enhanced emissions of both **74** and **75** were quenched drastically in the presence of PA (5 μM) in THF–H_2O (6 : 4) medium. Quenching efficiencies of nearly 67% for **74** and 96% for **75** were observed and the Stern–Volmer quenching constants were estimated to be 3.2×10^6 M^{-1} (**74**) and 2.0×10^6 M^{-1} (**75**). The authors proposed that the observed fluorescence quenching of sensor **74** followed the static-quenching mechanism in the ground state *via* hydrogen bonding interactions between –OH of PA and –NH_2 in **74**. On the other hand, **75** followed the charge-transfer quenching mechanism due to the lack of hydrogen-bonding interactions. The detection limits of **74** and **75** for PA were found to be 4 nM and 9 nM, respectively. Similar titrations of **74** and **75** with other interfering analytes such as 1,4-DNB, TNT, 2,4-DNT, 4-NT, NB, 2,3-dinitro-2,3-dimethyl butane (DNDMB) and BQ elicited very poor fluorescence quenching. 30 min exposure of aggregates of **74** and **75** to the PA vapor caused nearly 34% and 21% fluorescence quenching, respectively. Also, dip-coated paper-strips of **74** and **75** exhibited an attogram level of sensitivity for PA.[70]

A triptycene-based 3D nanographene **76** bearing three hexa-*peri*-hexabenzocoronenes (HBC) was synthesized and used as a selective fluorescent sensor for PA.[71] The unique 3D structural arrangements, due to the triptycene-scaffold of **76** displayed the intrinsic photoluminescence characteristics. The DCM solution of nanographene **76** showed a strong emission at 470 nm which was quenched upon addition of PA. The quenching efficiency was found to be 1.8×10^4 M^{-1} and the sensitivity was 2.4 ng mm^{-2}. Notably, similar titrations with other interfering analytes such as 2,4-DNP, 3-nitrophenol (3-NP), 4-NP, 3-nitrotoluene (3-NT), BA and phenol elicited very poor fluorescence quenching.[71]

11. Imidazolium based sensors

Imidazolium salts have been extensively used as ionic liquids and precursors in N-heterocyclic carbene (NHC) chemistry.[72] But their applications as sensors for anions, cations and small molecules, have drawn much attention in recent years owing to their water-soluble nature. In 2013, Mukherjee *et al.* have reported two anthracene-based tris-imidazolium salts (**77–78**) as fluorogenic sensors for PA in organic and aqueous media (Chart 12).[73] The X-ray diffraction analysis and DFT optimization defined that both sensors **77** and **78** adopted a *cis*,*cis*,*cis*-conformation to exhibit a bowl-shaped open cavity that could encapsulate the neutral NACs. Both **77** and **78** displayed a characteristic anthracene emission (at 399, 422 and 446 nm in DMSO) that was quenched rapidly upon addition of $CHCl_3$ solution of PA.

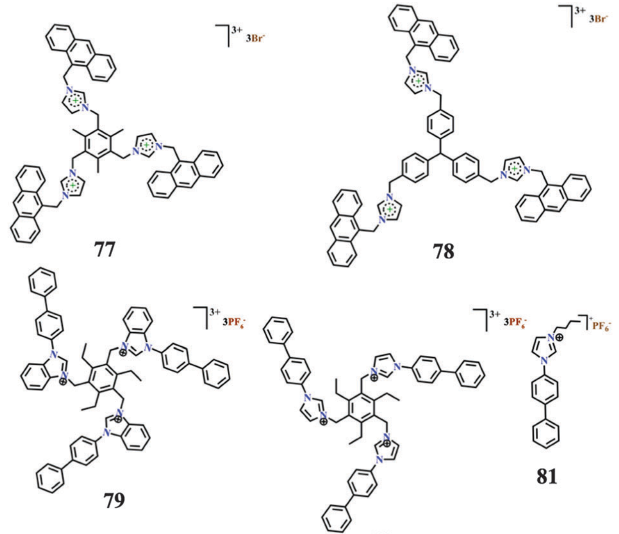

77 78 79 80 81

Chart 12 Imidazolium based molecular sensors for NACs.

The quenching efficiencies of **77** and **78** for PA were 92% and 91% and the detection limits were 467 and 354 ppb, respectively. The selectivity study indicated that both **77** and **78** elicited higher fluorescence quenching (K_{SV} = 3.8×10^4 M^{-1} for **77** and 3.3×10^4 M^{-1} for **78**) along with a marked visual color change from colorless to intense yellow only for PA, while other tested analytes induced a moderate to poor quenching effect (Fig. 8).

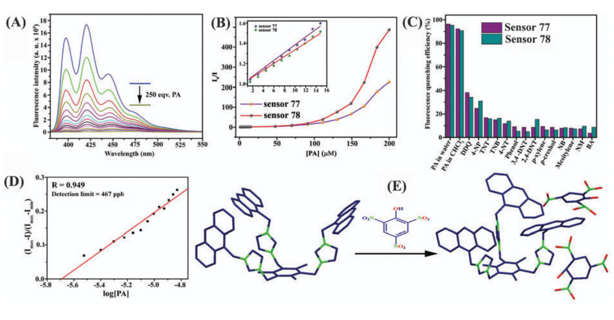

Fig. 8 (A) Reduction in fluorescence intensity of **77** upon gradual addition of PA. (B) Stern–Volmer plots for **77** and **78** using PA as a quencher (Inset: Stern–Volmer plots at lower concentration region of PA). (C) Fluorescence quenching efficiencies of **77** and **78** toward different analytes. (D) The detection limit plot of **77** for PA. (E) The molecular structure of **77** and its 1 : 2 host–guest complexation with PA in solid-state. Adapted with permission from ref. 73. Copyright 2013 American Chemical Society.

Despite their similar reduction potentials, the observed high fluorescence quenching for PA compared to TNT was ascribed to deprotonation of the phenolic –OH group followed by anion exchange from sensor molecules. The experimental (UV-vis, NMR and lifetime) results and DFT calculations revealed that the higher fluorescence quenching efficiency for PA followed an unusual ground-state electron-transfer from the picrate anion to the positively charged sensor. The ^{1}H NMR titration study confirmed the formation of 1 : 2 host–guest complexes between **77–78** and PA in solution and the same was unambiguously proved by solid-state by X-ray diffraction analysis of **77**.PA (Fig. 8).[73] Very recently, Kumar and co-workers have designed and synthesized two new (benz)Imidazolium based cavity controlled tricationic sensors **79–80** that provided both columbic and hydrogen-bonding interactions with negatively charged species including π–π interactions with electron-deficient analytes.[74] Due to steric gearing, the three alternate substituents pre-organized on the same side of the central triethylbenzene unit and provided the hydrophobic pocket capable of encapsulating NACs.

In fact, single crystal X-ray diffraction analysis revealed that sensor **80** adopts a *cis*,*cis*,*cis* conformation and three biphenyl substituents orient on the same side of the triethylbenzene plane to provide a pseudo hydrophobic cavity. To corroborate the role of the hydrophobic cavity in quenching efficiency, the authors also synthesized a monopod compound **81** as a reference sensor. The emission maximum of **79** at 470 nm was quenched rapidly and selectively upon increasing the quantity of PA, in HEPES buffer with 2% DMSO, along with a sharp visual color change. Upon addition of 50 mm concentration of different analytes, PA induced nearly 78% quenching, while moderate to poor (*ca.* 33% for 2,4-DNP, ~20% for 2-NP, ~12% for 2,4-DNT *etc.*) fluorescence quenching responses were observed upon addition of various other tested NACs. On the other hand, **80** (2 μM) displayed a similar fluorescence quenching pattern upon addition of 50 μM (25 equiv.) of various (nitro)aromatics. The poor selectivity of **80** surmised to the more flexible hydrophobic cavity that can be adjusted with respect to the size of analytes. The Stern–Volmer binding constants K_{SV} were 3.57×10^5 M^{-1} and 2.67×10^5 M^{-1} for **79** and **80**, respectively. The estimated quenching rate constant (2.12×10^6 ns M^{-1}) and unchanged fluorescence lifetime of **79** upon incremental addition of PA implied that fluorescence quenching predominantly followed the static mechanism. The non-linear regression analysis of the spectral data indicated the formation of 1 : 1 host–guest complexes between **79** or **80** with NACs. The significant upfield shift (Δδ = 0.8 ppm) of PA proton resonance in ^{1}H NMR titration studies suggested the encapsulation of PA in the cavity of **79** and **80** in solution. The DFT energy minimized structure of **79**. The picrate complex demonstrated that the oxygen atom of the picrate anion formed H-bonding interactions with C2–H protons of benzimidazloium moieties and *ortho*-nitro groups involved in H-bonding with either benzimidazloium C2–H or aryl C–H protons. The fluorogenic studies also showed that **79** can detect PA in water as low as 1.0 nM; but in contact-mode; **79** showed a detection limit of 137 ag cm^{-2} under UV light.[74]

12. Summary and outlook

In this review, we exemplified the recent noteworthy examples of small molecule based π-electron-rich turn-off fluorescent sensors used for nitroaromatic explosive detection. The synthetic

Table 1 Summary of sensing properties of small molecule sensors discussed in this article

Sensor	K_{SV} (M^{-1})	Analyte	Detection limit	Ref.
1	307–394	NACs	—	24
2	$1–3 \times 10^3$	NACs	—	25
3	1.4×10^3	TNT	ppb	26
4	1.9×10^2	TNT	—	27
5	6.4×10^3	TNT	—	27
6	6.6×10^4	TNT	ppb	28
7	8.4×10^4	TNT	ppb	28
8	2.9×10^5	TNT	—	29
9	4.0×10^6	PA	ppm	30
11	3.2×10^3	2-NP	ppm	32
12	9.9×10^3	PA	ppt	33
13	2.2×10^4	PA	ppt	33
14	1.1×10^3	PA	ppt	33
15	3.2×10^4	PA	ppt	33
16	8.1×10^3	PA	ppt	33
17	3.7×10^4	PA	ppt	33
18	5.0×10^4	TNT	ppb	29
19	5.0×10^4	TNT	—	35
20	2.6×10^5	TNT	—	35
21	4.0×10^5	TNT	ppb	35
22	1.4×10^5	TNT	—	35
27	8.7×10^4	TNT	ppb	27
28	2.1×10^3	PA	ppb	38
29	2.0×10^2	PA	ppb	38
30	1.3×10^2	PA	ppb	38
32	3.7×10^4	PA	—	40
35	1.3×10^6	TNT	ppb	43
36	1.0×10^6	TNT	ppb	43
37	1.6×10^7	PA	ppb	44
38	1.4×10^7	PA	ppb	44
39	7.2×10^2	DNT	—	45
41	9.9×10^4	PA	ppb	48
42	1.2×10^5	PA	ppb	49
43	1.5×10^4	PA	ppq	50
44	2.6×10^4	PA	ppq	50
45	5.4×10^4	PA	ppq	50
46	7.9×10^4	PA	ppq	50
50	3.3×10^3	TNT	—	53
56	2.9×10^5	PA	ppb	57
58	2.9×10^5	PA	ppb	58
59	4.4×10^3	PA	ppm	60
60	7.0×10^4	PA	ppm	61
61	8.4×10^2	TNT	—	62
62	7.2×10^2	TNT	—	62
63	1.7×10^3	TNT	ppb	62
64	6.4×10^3	TNT	—	62
65	2.9×10^6	PA	ppb	63
66	1.4×10^7	PA	ppb	63
67	1.8×10^5	PA	ppb	64
69	5.7×10^6	PA	ppb	65
71	2.9×10^5	PA	ppb	65
72	1.2×10^5	PA	—	67
73	3.8×10^5	PA	ppm	68
74	3.2×10^6	PA	ppb	70
75	2.0×10^6	PA	ppb	70
76	1.8×10^4	PA	ppb	71
77	3.8×10^4	PA	ppb	73
78	3.3×10^4	PA	ppb	73
79	3.5×10^5	PA	ppb	74
80	2.6×10^5	PA	—	74

simplicity, easy functionalization and wide-range sensing ability for chemical explosives, make the small molecule fluorophores promising sensory materials for NAC detection.[22] Furthermore, the high solubility of small molecule based fluorescent sensors in common solvents make them suitable for easy fabrication for the practical applications. The moderate to high quenching efficiency of electron-rich small molecule fluorescent sensors is attributed to their effective charge-transfer (donor–acceptor) complexation with electron-deficient nitroaromatic explosives (Table 1). However, despite their efficient sensing ability and high selectivity, small molecule fluorescent sensors are inferior compared to conjugated polymeric sensors. The conjugated polymeric sensors are highly efficient as several excitonic emissions can be quenched by one molecule of the quencher through long-range excitonic migration along the polymeric chain.[9g,52b,75] In contrast, the emission of small molecule sensors is quenched in a stoichiometric way of one fluorophore per analyte. One possible way to address this issue is to design supramolecular sensors by linking simple fluorophores through multiple supramolecular interactions.[13k,33,38] Therefore, the small molecule fluorophores can be viewed as leading compounds for further development of much improved fluorescent sensors by introducing suitable substituents or embedding them within a matrix that could enhance the binding efficiency between the sensors and explosives.[22a]

Acknowledgements

We sincerely thank all the co-workers who have contributed to the research as cited. Financial support from the Department of Science and Technology (India) is acknowledged.

Notes and references

1 D. Banerjee, Z. Hu and J. Li, *Dalton Trans.*, 2014, **43**, 10668–10685.

2 Y. Salinas, R. Martinez-Manez, M. D. Marcos, F. Sancenon, A. M. Costero, M. Parra and S. Gil, *Chem. Soc. Rev.*, 2012, **41**, 1261–1296.

3 (*a*) https://en.wikipedia.org/wiki/Tritonal; (*b*) http://science.howstuffworks.com/moab3.htm.

4 (*a*) S. Singh, *J. Hazard. Mater.*, 2007, **144**, 15–28; (*b*) S. Talmage, D. Opresko, C. Maxwell, C. E. Welsh, F. M. Cretella, P. Reno and F. B. Daniel, in *Rev. Environ. Contam T.*, ed. G. Ware, Springer, New York, 1999, vol. 161, pp. 1–156; (*c*) C. Vorbeck, H. Lenke, P. Fischer and H. J. Knackmuss, *J. Bacteriol.*, 1994, **176**, 932–934.

5 Environmental Protection Agency, innovative treatment technologies: Annual status report, 8th edn, 1996.

6 (*a*) K. Håkansson, R. V. Coorey, R. A. Zubarev, V. L. Talrose and P. Håkansson, *J. Mass Spectrom.*, 2000, **35**, 337–346; (*b*) D. S. Moore, *Rev. Sci. Instrum.*, 2004, **75**, 2499–2512; (*c*) R. D. Luggar, M. J. Farquharson, J. A. Horrocks and R. J. Lacey, *X-Ray Spectrom.*, 1998, **27**, 87–94.

7 (*a*) J. R. Lakowicz, *Principles of Fluorescence Spectroscopy*, Springer, 3rd edn, 2006; (*b*) T. W. Bell and N. M. Hext, *Chem. Soc. Rev.*, 2004, **33**, 589–598; (*c*) H. Lu, L. Xiong, H. Liu, M. Yu, Z. Shen, F. Li and X. You, *Org. Biomol. Chem.*, 2009, **7**, 2554–2558; (*d*) E. M. Nolan and S. J. Lippard, *Chem. Rev.*, 2008, **108**, 3443–3480; (*e*) A. P. de Silva, H. Q. N. Gunaratne, T. Gunnlaugsson, A. J. M. Huxley, C. P. McCoy, J. T. Rademacher and T. E. Rice, *Chem. Rev.*, 1997, **97**, 1515–1566; (*f*) S. J. Bradberry, A. J. Savyasachi, M. Martinez-Calvo and T. Gunnlaugsson, *Coord. Chem. Rev.*, 2014, **273–274**, 226–241; (*g*) W. Guan, W. Zhou, J. Lu and C. Lu, *Chem. Soc. Rev.*, 2015, **44**, 6981–7009.

8 (*a*) B. Tang, B. Ding, K. Xu and L. Tong, *Chem. – Eur. J.*, 2009, **15**, 3147–3151; (*b*) D. Samanta, S. Shanmugaraju, S. A. Joshi, Y. P. Patil, M. Nethaji and P. S. Mukherjee, *Chem. Commun.*, 2012, **48**, 2298–2300; (*c*) S. Shanmugaraju, A. K. Bar, H. Jadhav, D. Moon and P. S. Mukherjee, *Dalton Trans.*, 2013, **42**, 2998–3008; (*d*) S. Shanmugaraju, V. Vajpayee, S. Lee, K.-W. Chi, P. J. Stang and P. S. Mukherjee, *Inorg. Chem.*, 2012, **51**, 4817–4823; (*e*) S. Anbu, S. Shanmugaraju, R. Ravishankaran, A. A. Karande and P. S. Mukherjee, *Inorg. Chem. Commun.*, 2012, **25**, 26–29; (*f*) J. P. Byrne, J. A. Kitchen and T. Gunnlaugsson, *Chem. Soc. Rev.*, 2014, **43**, 5302–5325; (*g*) D. S. Kim and J. L. Sessler, *Chem. Soc. Rev.*, 2015, **44**, 532–546; (*h*) L. Xu, Y.-X. Wang and H.-B. Yang, *Dalton Trans.*, 2015, **44**, 867–890.

9 (*a*) S. Rochat and T. M. Swager, *ACS Appl. Mater. Interfaces*, 2013, **5**, 4488–4502; (*b*) J.-S. Yang and T. M. Swager, *J. Am. Chem. Soc.*, 1998, **120**, 11864–11873; (*c*) S. W. Thomas III, J. P. Amara, R. E. Bjork and T. M. Swager, *Chem. Commun.*, 2005, 4572–4574; (*d*) T. L. Andrew and T. M. Swager, *J. Am. Chem. Soc.*, 2007, **129**, 7254–7255; (*e*) S. Yamaguchi and T. M. Swager, *J. Am. Chem. Soc.*, 2001, **123**, 12087–12088; (*f*) A. Rose, Z. Zhu, C. F. Madigan, T. M. Swager and V. Bulovic, *Nature*, 2005, **434**, 876–879; (*g*) S. J. Toal and W. C. Trogler, *J. Mater. Chem.*, 2006, **16**, 2871–2883; (*h*) J. C. Sanchez and W. C. Trogler, *J. Mater. Chem.*, 2008, **18**, 3143–3156; (*i*) H. Sohn, R. M. Calhoun, M. J. Sailor and W. C. Trogler, *Angew. Chem., Int. Ed.*, 2001, **40**, 2104–2105; (*j*) H. Sohn, M. J. Sailor, D. Magde and W. C. Trogler, *J. Am. Chem. Soc.*, 2003, **125**, 3821–3830.

10 A. McCluskey, C. I. Holdsworth and M. C. Bowyer, *Org. Biomol. Chem.*, 2007, **5**, 3233–3244.

11 (*a*) Z. Hu, B. J. Deibert and J. Li, *Chem. Soc. Rev.*, 2014, **43**, 5815–5840; (*b*) S. S. Nagarkar, A. V. Desai, P. Samanta and S. K. Ghosh, *Dalton Trans.*, 2015, **44**, 15175–15180; (*c*) Y.-P. Xia, Y.-W. Li, D.-C. Li, Q.-X. Yao, Y.-C. Du and J.-M. Dou, *CrystEngComm*, 2015, **17**, 2459–2463; (*d*) C. Zhang, L. Sun, Y. Yan, J. Li, X. Song, Y. Liu and Z. Liang, *Dalton Trans.*, 2015, **44**, 230–236; (*e*) A. Mallick, B. Garai, M. A. Addicoat, P. S. Petkov, T. Heine and R. Banerjee, *Chem. Sci.*, 2015, **6**, 1420–1425; (*f*) R.-M. Wen, S.-D. Han, G.-J. Ren, Z. Chang, Y.-W. Li and X.-H. Bu, *Dalton Trans.*, 2015, **44**, 10914–10917; (*g*) J. Liu, S. Yang, F. Li, L. Dong, J. Liu, X. Wang and Q. Pu, *J. Mater. Chem. A*, 2015, **3**, 10069–10076; (*h*) L. Zhang, L. Sun, X. Li, Y. Tian and G. Yuan, *Dalton Trans.*, 2015, **44**, 401–410; (*i*) E. Cariati, E. Lucenti, C. Botta, U. Giovanella, D. Marinotto and S. Righetto, *Coord. Chem. Rev.*, 2015, DOI: 10.1016/j.ccr.2015.03.004; (*j*) S. Mukherjee, A. V. Desai, B. Manna, A. I. Inamdar and S. K. Ghosh, *Cryst. Growth Des.*, 2015, **15**, 4627–4634; (*k*) B. Joarder, A. V. Desai, P. Samanta, S. Mukherjee and S. K. Ghosh, *Chem. – Eur. J.*, 2015, **21**, 965–969; (*l*) M. Tu, S. Wannapaiboon, K. Khaletskaya and R. A. Fischer, *Adv. Funct. Mater.*, 2015, **25**, 4470–4479; (*m*) B. Gole, A. K. Bar and P. S. Mukherjee, *Chem. Commun.*, 2011, **47**, 12137–12139.

12 (*a*) G. Das, B. P. Biswal, S. Kandambeth, V. Venkatesh, G. Kaur, M. Addicoat, T. Heine, S. Verma and R. Banerjee, *Chem. Sci.*, 2015, **6**, 3931–3939; (*b*) C. Gu, N. Huang, Y. Wu, H. Xu and D. Jiang, *Angew. Chem., Int. Ed.*, 2015, DOI: 10.1002/anie.201504786; (*c*) X. Liu, Y. Xu and D. Jiang, *J. Am. Chem. Soc.*, 2012, **134**, 8738–8741; (*d*) G. Nagarjuna, A. Kumar, A. Kokil, K. G. Jadhav, S. Yurt, J. Kumar and D. Venkataraman, *J. Mater. Chem.*, 2011, **21**, 16597–16602; (*e*) L. Guo and D. Cao, *J. Mater. Chem. C*, 2015, **3**, 8490–8494.

13 (*a*) S. Ghosh and P. S. Mukherjee, *Organometallics*, 2008, **27**, 316–319; (*b*) S. Ghosh, B. Gole, A. K. Bar and P. S. Mukherjee, *Organometallics*, 2009, **28**, 4288–4296; (*c*) M. Wang, V. Vajpayee, S. Shanmugaraju, Y.-R. Zheng, Z. Zhao, H. Kim, P. S. Mukherjee, K.-W. Chi and P. J. Stang, *Inorg. Chem.*, 2011, **50**, 1506–1512; (*d*) A. K. Bar, S. Shanmugaraju, K.-W. Chi and P. S. Mukherjee, *Dalton Trans.*, 2011, **40**, 2257–2267; (*e*) S. Shanmugaraju, A. K. Bar, S. A. Joshi, Y. P. Patil and P. S. Mukherjee, *Organometallics*, 2011, **30**, 1951–1960; (*f*) V. Vajpayee, H. Kim, A. Mishra, P. S. Mukherjee, P. J. Stang, M. H. Lee, H. K. Kim and K.-W. Chi, *Dalton Trans.*, 2011, **40**, 3112–3115; (*g*) S. Shanmugaraju, S. A. Joshi and P. S. Mukherjee, *Inorg. Chem.*, 2011, **50**, 11736–11745; (*h*) S. Shanmugaraju, H. Jadhav, Y. P. Patil and P. S. Mukherjee, *Inorg. Chem.*, 2012, **51**, 13072–13074; (*i*) S. Shanmugaraju, H. Jadhav and P. Mukherjee, *Proc. Natl. Acad. Sci., India, Sect. A*, 2014, **84**, 197–203; (*j*) K. Acharyya and P. S. Mukherjee, *Chem. Commun.*, 2014, **50**, 15788–15791; (*k*) S. Shanmugaraju and P. S. Mukherjee, *Chem. – Eur. J.*, 2015,

21, 6656–6666; (*l*) E. Guzman-Percastegui, M. Vonlanthen, B. Quiroz-Garcia, M. Flores-Alamo, E. Rivera and I. Castillo, *Dalton Trans.*, 2015, **44**, 15966–15975; (*m*) A. Dubey, A. Mishra, J. W. Min, M. H. Lee, H. Kim, P. J. Stang and K.-W. Chi, *Inorg. Chim. Acta*, 2014, **423**(part A), 326–331.

14 (*a*) K. K. Kartha, A. Sandeep, V. K. Praveen and A. Ajayaghosh, *Chem. Rec.*, 2015, **15**, 252–265; (*b*) K. K. Kartha, A. Sandeep, V. C. Nair, M. Takeuchi and A. Ajayaghosh, *Phys. Chem. Chem. Phys.*, 2014, **16**, 18896–18901; (*c*) Y. Che, D. E. Gross, H. Huang, D. Yang, X. Yang, E. Discekici, Z. Xue, H. Zhao, J. S. Moore and L. Zang, *J. Am. Chem. Soc.*, 2012, **134**, 4978–4982; (*d*) B. Xu, Y. Xu, X. Wang, H. Li, X. Wu, H. Tong and L. Wang, *Polym. Chem.*, 2013, **4**, 5056–5059; (*e*) T. Naddo, Y. Che, W. Zhang, K. Balakrishnan, X. Yang, M. Yen, J. Zhao, J. S. Moore and L. Zang, *J. Am. Chem. Soc.*, 2007, **129**, 6978–6979; (*f*) C. Vijayakumar, G. Tobin, W. Schmitt, M.-J. Kim and M. Takeuchi, *Chem. Commun.*, 2010, **46**, 874–876.

15 (*a*) K. J. Albert and D. R. Walt, *Anal. Chem.*, 2000, **72**, 1947–1955; (*b*) J. Geng, P. Liu, B. Liu, G. Guan, Z. Zhang and M.-Y. Han, *Chem. – Eur. J.*, 2010, **16**, 3720–3727; (*c*) J. Yang, S. Aschemeyer, H. P. Martinez and W. C. Trogler, *Chem. Commun.*, 2010, **46**, 6804–6806; (*d*) S. Tao, J. Yin and G. Li, *J. Mater. Chem.*, 2008, **18**, 4872–4878; (*e*) S. Tao, G. Li and H. Zhu, *J. Mater. Chem.*, 2006, **16**, 4521–4528; (*f*) Y. Salinas, M. V. Solano, R. E. Sørensen, K. R. Larsen, J. Lycoops, J. O. Jeppesen, R. Martínez-Máñez, F. Sancenón, M. D. Marcos, P. Amorós and C. Guillem, *Chem. – Eur. J.*, 2014, **20**, 855–866; (*g*) Y. Salinas, A. Agostini, E. Perez-Esteve, R. Martinez-Manez, F. Sancenon, M. Dolores Marcos, J. Soto, A. M. Costero, S. Gil, M. Parra and P. Amoros, *J. Mater. Chem. A*, 2013, **1**, 3561–3564; (*h*) Y. Salinas, R. Martínez-Máñez, J. O. Jeppesen, L. H. Petersen, F. Sancenón, M. D. Marcos, J. Soto, C. Guillem and P. Amorós, *ACS Appl. Mater. Interfaces*, 2013, **5**, 1538–1543; (*i*) K. Sarkar, Y. Salinas, I. Campos, R. Martínez-Máñez, M. D. Marcos, F. Sancenón and P. Amorós, *ChemPlusChem*, 2013, **78**, 684–694.

16 (*a*) P. E. Shaw, S. S. Y. Chen, X. Wang, P. L. Burn and P. Meredith, *J. Phys. Chem. C*, 2013, **117**, 5328–5337; (*b*) G. Tang, S. S. Y. Chen, P. E. Shaw, K. Hegedus, X. Wang, P. L. Burn and P. Meredith, *Polym. Chem.*, 2011, **2**, 2360–2368; (*c*) V. Balzani, P. Ceroni, A. Juris, M. Venturi, S. Campagna, F. Puntoriero and S. Serroni, *Coord. Chem. Rev.*, 2001, **219–221**, 545–572.

17 (*a*) K. Zhang, H. Zhou, Q. Mei, S. Wang, G. Guan, R. Liu, J. Zhang and Z. Zhang, *J. Am. Chem. Soc.*, 2011, **133**, 8424–8427; (*b*) G. H. Shi, Z. B. Shang, Y. Wang, W. J. Jin and T. C. Zhang, *Spectrochim. Acta, Part A*, 2008, **70**, 247–252; (*c*) R. Freeman, T. Finder, L. Bahshi, R. Gill and I. Willner, *Adv. Mater.*, 2012, **24**, 6416–6421; (*d*) S. Xu and H. Lu, *Chem. Commun.*, 2015, **51**, 3200–3203.

18 (*a*) G. V. Zyryanov, D. S. Kopchuk, I. S. Kovalev, E. V. Nosova, V. L. Rusinov and O. N. Chupakhin, *Russ. Chem. Rev.*, 2014, **83**, 783; (*b*) N. Dey, S. K. Samanta and S. Bhattacharya, *ACS Appl. Mater. Interfaces*, 2013, **5**, 8394–8400; (*c*) J. S. Park, F. Le Derf, C. M. Bejger, V. M. Lynch, J. L. Sessler, K. A. Nielsen, C. Johnsen and J. O. Jeppesen, *Chem. – Eur. J.*, 2010, **16**, 848–854; (*d*) S. Chakravarty, B. Gogoi and N. Sen Sarma, *J. Lumin.*, 2015, **165**, 6–14; (*e*) M. Kandpal, A. K. Bandela, V. K. Hinge, V. R. Rao and C. P. Rao, *ACS Appl. Mater. Interfaces*, 2013, **5**, 13448–13456; (*f*) N. Venkatramaiah, C. F. Pereira, R. F. Mendes, F. A. A. Paz and J. P. C. Tomé, *Anal. Chem.*, 2015, **87**, 4515–4522; (*g*) A. Rana and P. K. Panda, *RSC Adv.*, 2012, **2**, 12164–12168; (*h*) L. Mosca, S. Karimi Behzad and P. Anzenbacher, *J. Am. Chem. Soc.*, 2015, **137**, 7967–7969.

19 (*a*) T. Caron, E. Pasquinet, A. van der Lee, R. B. Pansu, V. Rouessac, S. Clavaguera, M. Bouhadid, F. Serein-Spirau, J.-P. Lère-Porte and P. Montméat, *Chem. – Eur. J.*, 2014, **20**, 15069–15076; (*b*) Y. Zhao, W. Hao, W. Ma, Z. Zang, H. Zhang, X. Liu, S. Zou, H. Zhang, W. Liu and J. Gao, *New J. Chem.*, 2014, **38**, 5754–5760; (*c*) V. Bhalla, A. Gupta, M. Kumar, D. S. S. Rao and S. K. Prasad, *ACS Appl. Mater. Interfaces*, 2013, **5**, 672–679; (*d*) S. Kaur, A. Gupta, V. Bhalla and M. Kumar, *J. Mater. Chem. C*, 2014, **2**, 7356–7363; (*e*) V. Bhalla, A. Gupta and M. Kumar, *Org. Lett.*, 2012, **14**, 3112–3115.

20 (*a*) G. Sivaraman, B. Vidya and D. Chellappa, *RSC Adv.*, 2014, **4**, 30828–30831; (*b*) S. Madhu, A. Bandela and M. Ravikanth, *RSC Adv.*, 2014, **4**, 7120–7123; (*c*) R. Chopra, V. Bhalla, M. Kumar and S. Kaur, *RSC Adv.*, 2015, **5**, 24336–24341; (*d*) V. Nagarajan and B. Bag, *Org. Biomol. Chem.*, 2014, **12**, 9510–9513.

21 (*a*) N. Venkatesan, V. Singh, P. Rajakumar and A. K. Mishra, *RSC Adv.*, 2014, **4**, 53484–53489; (*b*) J.-H. Wang, H.-T. Feng and Y.-S. Zheng, *Chem. Commun.*, 2014, **50**, 11407–11410; (*c*) O. Pinrat, K. Boonkitpatarakul, W. Paisuwan, M. Sukwattanasinitt and A. Ajavakom, *Analyst*, 2015, **140**, 1886–1893; (*d*) A. Gupta, J. H. Lee, J. H. Seo, S. G. Lee and J. S. Park, *RSC Adv.*, 2015, **5**, 73989–73992; (*e*) C. A. Swamy and P. Thilagar, *Chem. – Eur. J.*, 2015, **21**, 8874–8882; (*f*) K. Boonkitpatarakul, Y. Yodta, N. Niamnont and M. Sukwattanasinitt, *RSC Adv.*, 2015, **5**, 33306–33311; (*g*) P. Lasitha and E. Prasad, *RSC Adv.*, 2015, **5**, 41420–41427; (*h*) V. Bereau, C. Duhayon and J.-P. Sutter, *Chem. Commun.*, 2014, **50**, 12061–12064; (*i*) K. Shiraishi, T. Sanji and M. Tanaka, *ACS Appl. Mater. Interfaces*, 2009, **1**, 1379–1382; (*j*) X. He, P. Zhang, J.-B. Lin, H. V. Huynh, S. E. Navarro Muñoz, C.-C. Ling and T. Baumgartner, *Org. Lett.*, 2013, **15**, 5322–5325; (*k*) J.-F. Xiong, J.-X. Li, G.-Z. Mo, J.-P. Huo, J.-Y. Liu, X.-Y. Chen and Z.-Y. Wang, *J. Org. Chem.*, 2014, **79**, 11619–11630.

22 (*a*) M. E. Germain and M. J. Knapp, *Chem. Soc. Rev.*, 2009, **38**, 2543–2555; (*b*) X. Sun, Y. Wang and Y. Lei, *Chem. Soc. Rev.*, 2015, DOI: 10.1039/C1035CS00496A.

23 (*a*) M. E. Germain, T. R. Vargo, P. G. Khalifah and M. J. Knapp, *Inorg. Chem.*, 2007, **46**, 4422–4429; (*b*) M. E. Germain and M. J. Knapp, *J. Am. Chem. Soc.*, 2008, **130**, 5422–5423; (*c*) P. Beyazkilic, A. Yildirim and M. Bayindir, *ACS Appl. Mater. Interfaces*, 2014, **6**, 4997–5004.

24 J. V. Goodpaster and V. L. McGuffin, *Anal. Chem.*, 2001, **73**, 2004–2011.

25 W. Chen, N. B. Zuckerman, J. P. Konopelski and S. Chen, *Anal. Chem.*, 2010, **82**, 461–465.

26 S. Shanmugaraju, S. A. Joshi and P. S. Mukherjee, *J. Mater. Chem.*, 2011, **21**, 9130–9138.

27 S. Shanmugaraju, H. Jadhav, R. Karthik and P. S. Mukherjee, *RSC Adv.*, 2013, **3**, 4940–4950.

28 N. Venkatramaiah, A. D. G. Firmino, F. A. Almeida Paz and J. P. C. Tome, *Chem. Commun.*, 2014, **50**, 9683–9686.

29 J.-H. Hong, J.-H. Choi and D.-G. Cho, *Bull. Korean Chem. Soc.*, 2014, **35**, 3158–3162.

30 D. Udhayakumari, S. Velmathi, P. Venkatesan and S.-P. Wu, *Anal. Methods*, 2015, **7**, 1161–1166.

31 T. Liu, K. Zhao, K. Liu, L. Ding, S. Yin and Y. Fang, *J. Hazard. Mater.*, 2013, **246–247**, 52–60.

32 P. Sam-ang, D. Raksasorn, M. Sukwattanasinitt and P. Rashatasakhon, *RSC Adv.*, 2014, **4**, 58077–58082.

33 B. Gole, W. Song, M. Lackinger and P. S. Mukherjee, *Chem. – Eur. J.*, 2014, **20**, 13662–13680.

34 M. Hardouin-Lerouge, P. Hudhomme and M. Salle, *Chem. Soc. Rev.*, 2011, **40**, 30–43.

35 S.-B. Kim, E.-B. Lee, J.-H. Choi and D.-G. Cho, *Tetrahedron*, 2013, **69**, 4652–4656.

36 S. K. Kim, J. M. Lim, T. Pradhan, H. S. Jung, V. M. Lynch, J. S. Kim, D. Kim and J. L. Sessler, *J. Am. Chem. Soc.*, 2014, **136**, 495–505.

37 Y. H. Lee, H. Liu, J. Y. Lee, S. H. Kim, S. K. Kim, J. L. Sessler, Y. Kim and J. S. Kim, *Chem. – Eur. J.*, 2010, **16**, 5895–5901.

38 B. Gole, S. Shanmugaraju, A. K. Bar and P. S. Mukherjee, *Chem. Commun.*, 2011, **47**, 10046–10048.

39 Y. Peng, A.-J. Zhang, M. Dong and Y.-W. Wang, *Chem. Commun.*, 2011, **47**, 4505–4507.

40 F. Zhang, L. Luo, Y. Sun, F. Miao, J. Bi, S. Tan, D. Tian and H. Li, *Tetrahedron*, 2013, **69**, 9886–9889.

41 (*a*) S. Shanmugaraju, A. K. Bar, K.-W. Chi and P. S. Mukherjee, *Organometallics*, 2010, **29**, 2971–2980; (*b*) S. Shanmugaraju, D. Samanta, B. Gole and P. S. Mukherjee, *Dalton Trans.*, 2011, **40**, 12333–12341; (*c*) G. Hong, J. Sun, C. Qian, P. Xue, P. Gong, Z. Zhang and R. Lu, *J. Mater. Chem. C*, 2015, **3**, 2371–2379.

42 K. S. Prakash and R. Nagarajan, *Tetrahedron*, 2013, **69**, 8269–8275.

43 M. Kumar, V. Vij and V. Bhalla, *Langmuir*, 2012, **28**, 12417–12421.

44 Z.-F. An, C. Zheng, R.-F. Chen, J. Yin, J.-J. Xiao, H.-F. Shi, Y. Tao, Y. Qian and W. Huang, *Chem. – Eur. J.*, 2012, **18**, 15655–15661.

45 C. Zhang, Y. Che, X. Yang, B. R. Bunes and L. Zang, *Chem. Commun.*, 2010, **46**, 5560–5562.

46 Z. Ding, Q. Zhao, R. Xing, X. Wang, J. Ding, L. Wang and Y. Han, *J. Mater. Chem. C*, 2013, **1**, 786–792.

47 Q. Yan, Y. Zhou, B.-B. Ni, Y. Ma, J. Wang, J. Pei and Y. Cao, *J. Org. Chem.*, 2008, **73**, 5328–5339.

48 N. Venkatramaiah, S. Kumar and S. Patil, *Chem. Commun.*, 2012, **48**, 5007–5009.

49 N. Venkatramaiah, S. Kumar and S. Patil, *Chem. – Eur. J.*, 2012, **18**, 14745–14751.

50 S. Kumar, N. Venkatramaiah and S. Patil, *J. Phys. Chem. C*, 2013, **117**, 7236–7245.

51 H. Xie, H. Wang, Z. Xu, R. Qiao, X. Wang, X. Wang, L. Wu, H. Lu and S. Feng, *J. Mater. Chem. C*, 2014, **2**, 9425–9430.

52 (*a*) FLIR; (*b*) T. M. Swager, *Acc. Chem. Res.*, 2008, **41**, 1181–1189.

53 G. V. Zyryanov, M. A. Palacios and P. Anzenbacher, *Org. Lett.*, 2008, **10**, 3681–3684.

54 P. Anzenbacher, L. Mosca, M. A. Palacios, G. V. Zyryanov and P. Koutnik, *Chem. – Eur. J.*, 2012, **18**, 12712–12718.

55 (*a*) S. Kohmoto, E. Mori and K. Kishikawa, *J. Am. Chem. Soc.*, 2007, **129**, 13364–13365; (*b*) H. Arora, V. Bhalla and M. Kumar, *RSC Adv.*, 2015, **5**, 32637–32642.

56 H. Wang, X. Xu, A. Kojtari and H.-F. Ji, *J. Phys. Chem. C*, 2011, **115**, 20091–20096.

57 V. Bhalla, H. Arora, H. Singh and M. Kumar, *Dalton Trans.*, 2013, **42**, 969–974.

58 V. Bhalla, H. Singh, M. Kumar and S. K. Prasad, *Langmuir*, 2011, **27**, 15275–15281.

59 S. Anbu, S. Shanmugaraju, R. Ravishankaran, A. A. Karande and P. S. Mukherjee, *Dalton Trans.*, 2012, **41**, 13330–13337.

60 M. Alfonso, A. Espinosa, A. Tárraga and P. Molina, *ChemistryOpen*, 2014, **3**, 242–249.

61 Z. Zhao, J. Liu, J. W. Yip Lam, C. Y. K. Chan, H. Qiu and B. Z. Tang, *Dyes Pigm.*, 2011, **91**, 258–263.

62 N. Niamnont, N. Kimpitak, K. Wongravee, P. Rashatasakhon, K. K. Baldridge, J. S. Siegel and M. Sukwattanasinitt, *Chem. Commun.*, 2013, **49**, 780–782.

63 L. Wenfeng, M. Hengchang and L. Ziqiang, *RSC Adv.*, 2014, **4**, 39351–39358.

64 P. B. Pati and S. S. Zade, *Tetrahedron Lett.*, 2014, **55**, 5290–5293.

65 A. Chowdhury and P. S. Mukherjee, *J. Org. Chem.*, 2015, **80**, 4064–4075.

66 D. Samanta and P. S. Mukherjee, *Dalton Trans.*, 2013, **42**, 16784–16795.

67 P. Vishnoi, M. G. Walawalkar, S. Sen, A. Datta, G. N. Patwari and R. Murugavel, *Phys. Chem. Chem. Phys.*, 2014, **16**, 10651–10658.

68 (*a*) P. Vishnoi, S. Sen, G. N. Patwari and R. Murugavel, *New J. Chem.*, 2015, **39**, 886–892; (*b*) P. Vishnoi, M. G. Walawalkar and R. Murugavel, *Cryst. Growth Des.*, 2014, **14**, 5668–5673.

69 K. S. Raja, S. Ramakrishnan and V. A. Raghunathan, *Chem. Mater.*, 1997, **9**, 1630–1637.

70 V. Vij, V. Bhalla and M. Kumar, *ACS Appl. Mater. Interfaces*, 2013, **5**, 5373–5380.

71 P.-C. Zhu, L.-N. Luo, P.-Q. Cen, J.-T. Li and C. Zhang, *Tetrahedron Lett.*, 2014, **55**, 6277–6280.

72 K. M. Hindi, M. J. Panzner, C. A. Tessier, C. L. Cannon and W. J. Youngs, *Chem. Rev.*, 2009, **109**, 3859–3884.

73 B. Roy, A. K. Bar, B. Gole and P. S. Mukherjee, *J. Org. Chem.*, 2013, **78**, 1306–1310.

74 R. Kumar, S. Sandhu, P. Singh, G. Hundal, M. S. Hundal and S. Kumar, *Asian J. Org. Chem.*, 2014, **3**, 805–813.

75 (*a*) S. W. Thomas, G. D. Joly and T. M. Swager, *Chem. Rev.*, 2007, **107**, 1339–1386; (*b*) B. Gole, A. K. Bar and P. S. Mukherjee, *Chem. – Eur. J.*, 2014, **20**, 13321–13336; (*c*) B. Gole, A. K. Bar and P. S. Mukherjee, *Chem. – Eur. J.*, 2014, **20**, 2276–2291.